AD-A051 539 VIRGINIA POLYTECHNIC INST AND STATE UNIV BLACKSBURG --ETC F/G 20/4
EXPERIMENTAL INVESTIGATION OF UNSTEADY SEPARATION.(U)
JAN 78 D P TELIONIS, C A KOROMILAS DAHC04-75-G-0067

UNCLASSIFIED ARO-12680.4-E NL

1 OF 1
ADA
051539

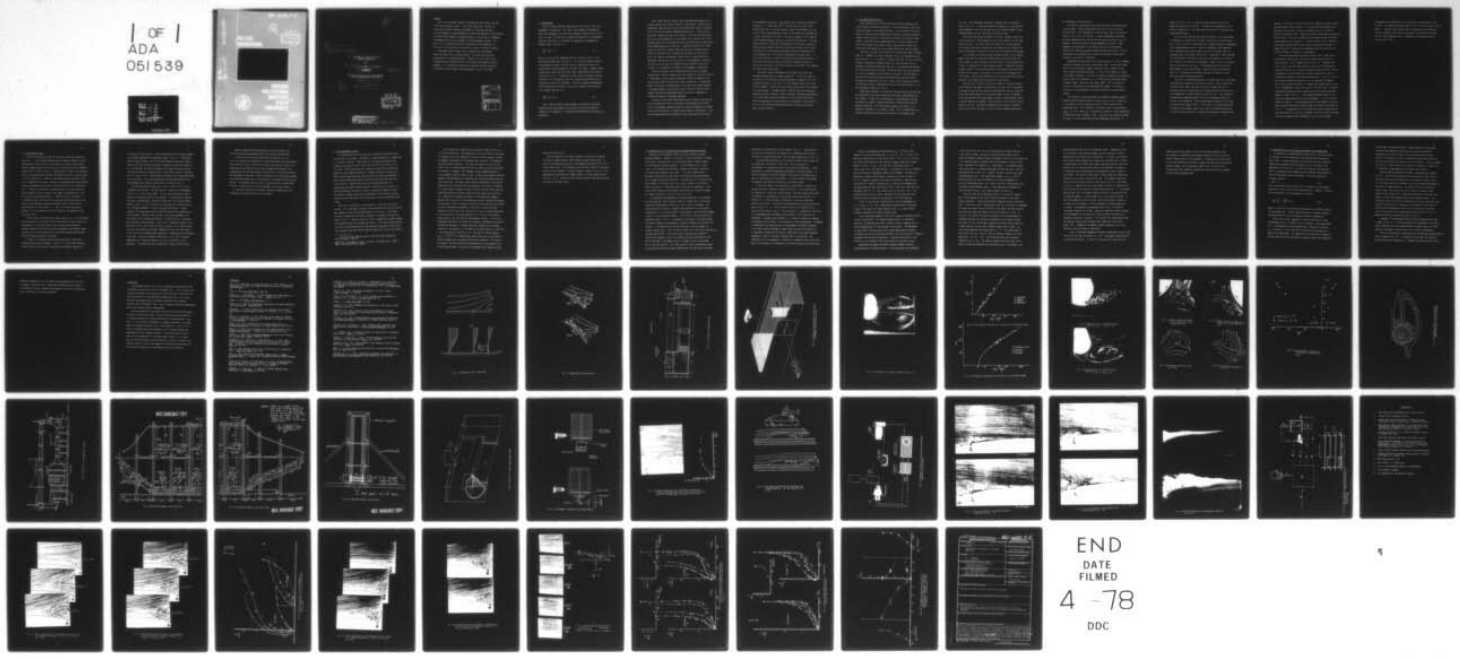

END
DATE
FILMED
4-78
DDC

COLLEGE OF ENGINEERING

VIRGINIA POLYTECHNIC INSTITUTE AND STATE UNIVERSITY

(1)

(9) Technical rept.,

(6) EXPERIMENTAL INVESTIGATION OF UNSTEADY SEPARATION.

BY

(10) D. P. Telionis and C. A. Koromilas

(11) January 1978

(12) 65 p.

Preliminary Report on U.S. Army Research Office Grant No. DAHC04-75-G-0067

(15)

(16) ARO (19) 12689.4-E

406 822

Preface

This is a preliminary report on the ARO Grant that carries the same title with the present report. The project essentially involves the setting up of special laboratory equipment to investigate unsteady viscous phenomena and the development of appropriate methods of visualization. Our efforts were plagued by unexpected delays in the arrival of equipment, a phenomenon certainly not uncommon for new experimental efforts. As a result a 5 or 6 month delay will be inevitable for the completion of this work. This extension of the effort is actually a no-cost extension.

The present report contains only a sample of our experimental results and some initial interpretations. A lot more data have been collected and is now being processed. Moreover, we are in the process of generating more information and in fact beyond the schedule originally proposed. It is expected to complete this phase of the work around May of 1978 and the final report can be completed in June or July 1978.

1. Introduction

One of the most important characteristics of viscous flow is the phenomenon of separation. This term in the language of aerodynamics means the breakaway of the flow from a bounding surface and the initiation of a wake. For the case of steady two-dimensional or axisymmetric flow over fixed walls, a criterion for separation was suggested by Prandtl (1904) (see Fig. 1.1)

$$\frac{\partial u}{\partial y} = 0 \text{ at } y = 0 \qquad (1)$$

where u is the velocity component parallel to the wall and y is the coordinate perpendicular to the wall. This criterion proved to predict the phenomenon correctly and thus has been used extensively by both theoreticians and experimentalists for over fifty years. However, Sears (1956) Moore (1958), and Rott (1956, 1964), demonstrated that Prandtl's criterion (Eq. (1)) is inadequate for cases other than steady flow over fixed walls and indicated the need for a generalized definition and a convenient criterion for separation. They also suggested independently a more appropriate criterion for the case of steady flow over moving walls, namely (see Fig. 1.2)

$$\frac{\partial u}{\partial y} = 0 \text{ at } u = 0 \qquad (2)$$

Sears (1956) and Moore (1958) proposed a definition of unsteady separation which are essentially equivalent to the above condition (equation (2)) expressed in a coordinate system moving with the point of separation.

Vidal (1959) and later Ludwig (1964) performed experiments with a cylinder rotating in the test section of a wind tunnel. Using hot wire anemometers, they were able to verify the theoretical model of equation (2) at least for the case of downstream moving walls. Tennant and his associates (Tennant and Yang, 1973; Tennant, 1973) also performed experiments with moving boundaries for both laminar and turbulent flow. Their findings pertain to skin velocities much larger than the free stream and always downstream motion of the skin. Despard and Miller (1971) again inspired by the work of Moore (1958) and the work of Sandborn and Liu (1968) for turbulent flow, considered the problem of an oscillating outer flow velocity and proposed a definition for a mean location of separation. Working with air and using hot wire anemometers, they were also able to verify that in unsteady flow the location of zero skin friction is not necessarily related to the phenomenon of separation.

Telionis and Werle (1973) showed analytically that for steady boundary-layer flow over moving walls, the location of zero skin friction is nonsingular, while a typical separation singularity appears at the station where Moore, Rott and Sears predict separation. A substantial number of analytical investigations on the topic have already appeared as reviewed recently by Sears and Telionis (1975) and Williams (1977). However the available experimental data up to now is inadequate to validate the models of unsteady separation.

The work of Vidal and Ludwig pertains only to steady flow, and the work of Despard and Miller is confined to high frequency oscillatory flow. Our knowledge, therefore, about this complex phenomenon is remarkably narrow and seriously in need of more intensive investigation. This can be accomplished both by methods of flow visualization, and by hot

wire anemometer techniques. Such methods have already been employed by Schraub et. al. (1956) Werle (1971), Ruiter, Nagib and Fejer (1971) and McCroskey (1971) to study unsteady viscous flow phenomena, but the specific cases considered and the scale of the models were designed for a study of the whole flow field. There was no emphasis on the features of the unsteady boundary-layer and in particular separation. In a most recent effort Carr, McAlister and McCroskey (1977) employ a variety of sensing devices ranging from flow visualization methods (tufts, smoke) to pressure or velocity measuring methods (pressure transducers, hot wire anemometers etc.) to study the phenomenon of unsteady stall. In this study some basic features of unsteady separation were verified. In particular pressure and velocity signatures throughout a period of oscillation are given for different stations on the airfoil and compared with flow visualization data.

The present authors attempted to investigate more closely the immediate neighborhood of unsteady separation. In the first phase of the work which is expected to be soon completed the emphasis is on the qualitative aspects of the flow. This was accomplished by flow visualization methods. Steady flows over moving surfaces were first examined in an open channel. Unsteady effects, transient and oscillatory were conducted with two different systems of pressure disturbance generations. In this preliminary report the reader will find a description of the facilities designed and constructed for this research, a description of the flow visualization methods developed and a sample of the experimental results received.

2. The Open Channel Facility

Open channel flow facilities offer some distinct advantages over closed tunnels, essentially because it is very convenient to insert and secure the models in the propoer position. In our particular case the models or other auxiliary equipment are required to perform some type of dynamic motion, and this is particularly difficult to achieve in water tunnels. The open facility appeared further to be very attractive in the initial phase of our project, when a large number of models and shapes had to be tested until the optimum combination could be chosen.

The flow is driven in this facility by a centrifugal pump (Fairbanks, Morse Co., 1160RPM, 4"ϕ) which discharges into a 18 cm diameter plastic pipe (see Fig. 2.1). This pump is certainly not ideal for such a facility because it generates an unwanted head, but it was available in the Engineering Science and Mechanics shop and its use appeared satisfactory for the initial steps of our work. Artificial head loses were provided by a valve, connected at the discharge of the pump. The pipe directs the flow into an open container where perforated sheets and screens eliminate the large scale vorticity. After a small converging section, the flow goes through a honeycomb and into the test section which is an open rectangular section 47 x 31 cm.

Models were inserted in the middle of the open section and the flow was visualized at the free surface or at horizontal planes beneath the free surface. Surface flow visualization is straightforward and does not require any special lighting facilities or particles with special buoyancy properties. For visualization beneath the surface, it is necessary to generate a flat sheet of light. This is accomplished by a system of lenses and a narrow slot on the wall of the channel (see

Fig. 2.2). The photographic equipment is mounted above the channel as shown in Fig. 2.2. A 16 mm movie camera with speeds up to 80 frames per second (AROFLEX-S) and a 35 mm motor drive still camera (NIKON-F2) with a MICRO-NIKKOR 55 mm lens, were used to record the flow.

Flow visualization was achieved at first with hydrogen bubbles and pliolite particles. These methods did not prove convenient for our open channel facility. The first, due to the necessity of special designs for locating wires next to moving walls, the second due to problems with proper lighting and visualization accross the free surface of the medium.

In this phase of our work we were interested mostly in low Reynolds number flows and such flows were accomplished with water-glycerin mixtures. However it was discovered that such mixtures quickly become milky if they are subjected to violent turbulent motion. Indeed the flow goes through a region of strong forced mixing in the pump and the valve that follows and this makes it very hard to visualize the flow beneath the free surface. Most of the experiments with glycerin-water mixtures were performed with surface pellets and surface visualization.

The flow over a circular cylinder was chosen for two basic reasons. On one hand the flow about a fixed circular cylinder is well documented and comparison with earlier analytical and numerical results is possible. On the other hand rotation of the cylinder about its axis of symmetry leaves the potential flow undisturbed, at least if the secondary effects of wake distortion are ignored. The skin motion is then the only disturbance of the flow. Any other configuration would require a system of belts on the skin of the body in order to achieve boundary motion with

no disturbance of the outer flow.

The flow was visualized on the surface with dyes injected upstream of the cylinder. Black buoyant pellets were also used to visualize particle paths. Still photographs of the flow were taken with exposure times of 1/2, 1/4 sec. and 1/8 sec. In these photographs established dye paths appeared clearly marking the wake region as shown in Fig. 2.3. Moreover, the pellets appear as shaded segments on the film. These segments are proportional to the average velocity of the particle, provided the streamline curvature effects are not very strong. All the experiments were performed with a 50-50% water-glycerin mixture which achieves a viscosity of 7 centipoise.

Experiments were performed with a fixed cylinder of 11 cm in diameter in order to compare with earlier experimental data. It should be noted that for the low Reynolds numbers tested, the wake is made up of two finite closed recirculating bubbles. In Fig. 2.4 we compare the length of the wake as measured in our flow visualization pictures with theoretical results compiled by Pruppacher et. al. (1970) and the experimental data of Homann (1936), Fage (1934) and Taneda (1956). Fig. 2.5 shows the location of separation for different Reynolds numbers. The present results are in good agreement with earlier analytical and experimental results.

The flow over a rotating cylinder was studied for Reynolds numbers ranging from 35 to 600 and velocity ratios u_w/U_∞ = 0.4 to 1.4 where u_w is the velocity of the cylinder skin and U_∞ is the velocity of the undisturbed flow. This corresponds to velocity ratios of approximately u_w/U_e = 0.2 to 0.7 where U_e is the outer flow velocity in the neighborhood of separation, that is around $\Theta = 90°$. The wake of the rotating cylinder for u_w/U_∞ = 0.8 with separation over the downstream moving wall, is

shown in Fig. 2.8. Fig. 2.7 shows the other side where the flow is opposed by the motion of the skin. The immediate neighborhood of the points of separation is visualized better by shorter film exposures and larger magnification.

Figs. 2.8b and 2.9b show the streamline pattern in the neighborhood of separation as received from the flow visualization of Figs 2.8a and 2.9a. Figs. 2.6 and 2.8 indicate that the streamline pattern of separation over a downstream moving wall is that of a saddlepoint and separation may be defined as the location where the velocity vanishes, that is a stagnation point exists away from the wall. Separation is then displaced in the direction of the motion of the skin with respect to its fixed-wall location. The separation displacement is shown in Fig. 2.10 plotted against the velocity ratio u_w/U_∞. The agreement with the results of other methods is quite satisfactory. However the aim of the present work is to illucidate the qualitative features of separation and no effort was made to generate more data.

The case of an upstream moving wall has always been very controversial and perhaps the problem has not yet been resolved. Moore (1958), Rott and Sears (Rott, 1964) argue that the point of separation over an upstream moving wall should again be a stagnation point and such that in its neighborhood, the same criterion is met (Eq. (2)). The streamline configurations suggested however, are not in agreement as Sears and Telionis (1975) emphasize. Earlier experimental evidence on the topic are inconclusive (Ludwig, 1964). In this work it is explained that the thickness of the boundary layer on the side of an upstream moving wall is very large and a sublayer is present which appears to be coming from

the wake. As a result, it was not possible to check the singular profile assumed by Moore, Rott and Sears. It is clear that the boundary layer equations do not accept a solution that meets the M.R.S. criterion (Fansler and Danberg, 1976). However this does not exclude the possibility that the M.R.S. condition is actually met and therefore that the Navier Stokes equations could capture it. In fact Tsahalis' (1976) numerical calculations indicate that for the case of an upstream moving wall, it appears that M.R.S. conditions are approached with the same rate with which the Goldstein singularity is approached.

The present experimental evidence indicates that a saddle point configuration exists on the side of the cylinder where the wall is moving upstream. This is shown clearly in Fig. 2.9. Therefore, the fluid in one of the four areas defined by the critical streamlines is moving with the wall in a direction opposite to the outer flow. This is in agreement with the observation of Ludwig who describes it as "a sublayer which appears to be coming from the wake." In fact it is felt that Ludwig's discovery should not at all be considered an anomaly. Such a layer would be necessary if a saddle-point pattern were to exist in this neighborhood as Sears and Telionis (1975) point out. An overall flow pattern emerges now which together with the distorted separation bubbles is shown in Fig. 2.11. The streamline pattern shown in this figure was always observed during our experiments. It was not too convenient to capture it in one photograph but piecing together the information received from smaller frame pictures we arrived at the sketch of Fig. 2.11. The geometry of this figure may not be very accurate but on the other hand this is not just a schematic of the flow field. The error involved in sketching these streamlines, that is their sidewise

displacement, was estimated to be less than 10% of the diameter of the cylinder. The streamline pattern shown in Fig. 2.11 has only two critical points. It appears that the upper point of separation has merged with the rear stagnation point and the lower point of separation has merged with the front stagnation point in agreement with the description of Telionis (1970, 1976).

3. The VPI Water Tunnel

The basic specifications that the VPI water tunnel was expected to meet were: a. Test sections appropriate for studying laminar or turbulent boundary layers as well as the potential flow about single models. Reynolds numbers based on the length of the test section should therefore range from 10^4 to 10^6 or more; b. Lowest possible volume so that expensive fluids like glycerin-water mixtures, Dow-Corning Fluid etc. could be used to fill the facility; c. Materials that would sustain corrosive fluids as for example NaCl solutions, necessary for hydrogen-bubble visualization, potassium permanganate and dilute acidic solutions for dye visualization etc. It should be noted that no permanent dyes can be used, since the working medium is usually expensive and cannot be disposed after a set of dye visualization experiments; d. Operation free of vibrations. It is imperative that vibrations from the pump and the driving motor or any device used to generate unsteady hydrodynamic effects should not be transferred to the test section; e. Total cost within the order of $15,000. This task appeared difficult to meet due to unexpected rises of material costs.

To meet these specifications the tunnel shown in Fig. 3.1 was designed. Long and carefully calculated diffusers were avoided in order to meet the requirements of low cost and small total volume of working medium. Synthetic materials resisting the corrosive chemicals were chosen, namely plexiglass for the test sections and the settling chamber and PVC pipes for the remaining sections of the tunnel.

A circular to rectangular converging section leads to the short diffuser and the settling chamber. (see Fig 3.1) Guide vanes situated in the diffuser cut the size of large eddies and suppress separation

on the walls of the diffuser. At the upstream end of the settling chamber two aluminum honeycombs are situated as shown in Fig. 3.1. These honeycombs are made by Hexcel - Bel Air and have hexagonal openings of approximately 3 cm^2 cross-sectional area and a diameter to length ratio equal to 15. The diffuser, the settling chamber, the converging section and the test sections were all constructed out of plexi-glass pieces of dimensions (3/4 in x 4 ft x 8 ft). A great effort was made to avoid large deflections of the side walls. This was accomplished by prestressed external steel reinforcements and tranverse aluminum bolts as shown in Fig. 3.2.

The converging section leads into a 25 cm x 30 cm (10 in x 12 in) rectangular test section. The test section is made up of interchangable units of 2,7 m (9 ft) total length. In this way large Reynolds numbers with not so large velocities can be achieved. A flexible shoot leads the flow into a low-head pump. The pump is made by Bell and Gossett (model: VSCS-PF, S&D 12 x 14 x 12 1/2) and has the following basic characteristics: 12 in discharge diameter, 8 ft head, and 2000 gpm flowrate. Chrome coating of the pump housing and the impeller appeared very expensive and time consuming. Instead it was decided to have these components cold-galvonized by the Livingstore Coating Co. of North Carolina. Two motors are available to drive the pump. The first is a "Marathon Electric" 1170 RPM, 230V, 15 H.P. motor which can drive the system at full speed (3m/sec). To control the speed of the tunnel a DURCO BL-311 cast iron valve with a teflon lining and a stainless steel butterfly is connected to the discharge of the pump. For the low range of velocities a 2 H.P., 220 V variable speed motor (U.S. Electrical Motors with a U.S. varidrive) is also available. This motor can drive the pump with a range of 292-1170 RPM.

Elbows, transitions from rectangular to circular sections and returning pipes were manufactured out of PVC (Poly-Vinyl-Chloride).

A smaller facility was also constructed as shown in Fig. 3.3. This is a closed circuit tunnel with a free surface above the test section. The principle of such a facility is that the test section is totally submerged but the driving of the flow can be accomplished through a low speed impeller at the free surface of the facility. This facility offers the advantages of very small volume of contained fluid, convenient exchange of the working mediums and as a result, access to the model and the sensing devices. The same test section from our larger facility is received and therefore, preliminary tests can be performed with the small tunnel.

In the final version of this report, extensive information on the calibration of both facilities will be included.

4. The Experimental Lay-Out

To visualize the flow we use pliolite and amberlite particles* that are dispersed in the fluid. The density of these substances is respectively ρ = 1.02 and 1.05 g/cm^3. These particles are separated through sieve-screening, according to their sizes, into particles of the order of 0.1 to 0.5 mm. Pliolite particles are bright white and should be preferred because of their higher reflectivity. However mixtures of glycerin and water are more dense than pure water and pliolite particles dispersed in such mixtures experience buoyancy forces that push them toward the top of the facility. Amberlite particles were proved more useful for experiments with glycerin-water mixtures. The particles to be used in a certain experiment are mixed in vertical columns and allowed to settle. The neutrally buoyant particles are withdrawn from the mixture, leaving behind the ones that either float to the top or sink to the bottom of the column.

The flow is visualized in planes parallel to the axis of the test section. All of the models tested are two-dimensional and the test section was scanned to check the two-dimensionality of the flow. A thin sheet of light is generated by a system of lenses or a parabolic reflector as shown in Fig 4.1. The nearly parallel light so generated is passed through two successive slots of 5 mm width and then it is led into the test section. In front of the reflecting mirror and along the light path a flash bulb is also situated, which may flash through the same slots into the test section.

---

*Pliolite is the commercial name of polyvinyltoluene butadiene, made by Goodyear Chemicals.

Amberlite is the commercial name of a white ion exchange resin, IRA-93 made by the Rohm and Haas Company.

Still pictures are taken with a 35 mm Olympus Camera and a 90 m; f, 2.8 Vivitar Macro Lens. Time exposures of 1/2 up to 1/120 sec. are used. The images of particles expose the film over the time exposure interval by segments proportional to the average local velocity. This method of course has some limitations. The larger the speed of a particle, the shorter time its image exposes the film at a certain point and therefore the contrast is reduced. This drawback could be compensated only if a very powerful source of light is used. It was also discovered that the method is not appropriate for recording flow fields with both large and small velocities. The proper camera speed is determined by the order of magnitude of the velocities that are expected in the region of interest. If a camera speed is chosen to reveal the small-velocity fields then the faster moving particles expose almost the entire width of the film and it is impossible to measure the lengths of individual path segments. Moreover the direction of the instantaneous velocity cannot be calculated with accuracy, since for unsteady flows the particle paths do not coincide with the instantaneous streamlines of the flow. Finally, the most important criticism may arise from the fact, that for large accelerations of the flow and for long time exposures (1/2, 1/4 sec.), the average velocity may be very far from the instantaneous velocity. For all the experiments performed, this effect was carefully considered and the error involved was estimated. A typical length for changes due to unsteady diffusion is the quantity $L_d = \sqrt{\nu t}$ whereas the path traveled by a particle in the same period of time is $L_p = Ut$. The ratio of the two lengths $L_d/L_p = (\nu/U^2 t)^{1/2}$ is a dimensionless number indicative of the relative order of changes due to unsteady diffusion and convection. The smaller this number, the more accurate the representation of the unsteady flow by the present method. In most of our experiments this number was kept

below the value of 0.05.

With the opening of the camera shutter, a flash may be triggered to direct an intense beam of light through the same optical path. In this way the beginnings of particle path segments are marked on the film with brighter spots. This technique is particularly helpful if reversing flows are to be examined. A typical example is shown in Fig. 4.2. This photograph was received with a camera speed of 1/8 and a magnification ratio of 1 ÷ 2.5. Velocity profiles were constructed from these data and are shown on the same figure.

5. Separation Over a Fixed Surface With Unsteady Pressure Gradients

Separation of the boundary layer is usually induced by adverse pressure gradients. However, its location is almost unaffected by changes of the outer flow conditions if the body configuration induces regions of strong adverse pressure gradients. In the extreme case of a sharp corner, as for example the flow over a backward facing step, separation is located almost always at the corner. A lot more interesting for practical applications are the cases of mild adverse pressure gradients, as for example the flow over airfoils. In these cases it is possible that minor changes of the outer flow, like a small increase of the angle of attack, may result in large excursions of the point of separation. This implies large changes of the pressure distribution and therefore changes of integral quantities like airfoil drag, lift, etc.

To investigate the phenomenon of unsteady separation it was decided first to design an ideal situation, where for steady flows, two distinct locations of separation at points say I and II could be achieved. The flow would then be forced to readjust from conditions I to conditions II impulsively, or in a transient manner or continuously, back and forth between I and II, in an oscillatory fashion. To this end a circular section with dimensions given in Fig. 5.1 is attached at the bottom of the test section. This model is made out of plexiglass, to permit lighting of the flow on its surface. A 7 mm deep hole was drilled and later filled with epoxy, to provide a length scale. This is shown in almost all of the flow visualization pictures that follow. It was later used to calculate the lengths of particle path segments as well as to define the axial coordinates on the skin of the body. The boundary layer is allowed to grow on the bottom wall of the test section. It is then led over a small accelerating region, at the forward portion and towards separation at the lee side of our model.

Separation is controlled by a flap as shown in Fig. 5.1. Two positions of the flap are found that, for steady flow, correspond to two distinct locations of separation positions I and II shown schematically in Fig. 5.1.

The experiments described in this section with the fixed circular arc just described, correspond to flows over fixed surfaces, while unsteadiness is introduced via outer flow pressure distributions. In the next section we describe experiments performed with moving surfaces. In the first category we simulate changes of the airfoil environment due to gusts or other outer flow disturbances. The second category corresponds to changes of the angle of attack of an oscillating blade.

In the first phase of our experiments, using water as a medium, we examine the case of impulsive changes of the flow. To this end the flap is connected to a lever and a strong spring. With the release of the lever a microswitch is activated and a flap quickly moves from position I to position II. A simple system of electronics is used to activate the camera and the flash. This was first accomplished using a delay-circuit as shown in Fig. 5.2. It is thus possible to control the opening and the closing of the camera's shutter. The time delay, Δt , between the initiation of the phenomenon and the opening of the shutter is controlled and the experiment is repeated with different Δt in order to receive the sequence of unsteady velocity fields. This system has a clear disadvantage. A sequence of photographs thus generated does not correspond to different instances of the same transient phenomenon, spaced apart by equal time intervals Δt. It represents instead the flow field of repetitions of the same transient phenomenon, viewed at different instances after its initiation. The repeatability of the phenomenon is therefore an important factor and in fact some of the sequences of photographs thus received indicate discontinuities.

One set of experiments was performed with $R_e = 10^4$ and a sharp change of the flap inclination from $\theta_I = 0$ to $\theta_{II} = 40°$. In Fig. 5.3 we show four visualizations of the flow at times t = 0.2, 0.4, 0.6, and 0.8 sec. after the initiation of the impulsive change, taken with a camera speed of 1/8 sec. For $R_e \approx 10^4$, the flow is turbulent and this is clearly seen in all the visualizations. The sequence in Fig. 5.3 indicates that the location of separation, moves slowly upstream. The station of separation in these visualizations is marked by an arrow as shown in Fig. 5.3. However, upstream of the point of separation, there exists a relatively thin region of reversed flow, in qualitative agreement with the descriptions of Sears and Telionis (1971, 1975), Carr, McAlister and McCroskey (1977) et. al. (see review article of Telionis, 1977). The reversed direction of the flow is apparent from the bright dots that mark the particle location at the beginning of the film exposure.

In Fig. 5.4 we show dye visualization of the same phenomenon for $\Delta t = 0.2$ and $\Delta t = 0.5$. Dye is emmitted here approximately 10 mm downstream of the location of steady separation and it is seen to creep upstream, underneath the laminar boundary layer.

A very interesting feature of the flow is apparent from both particle and dye visualization. The separated region grows in a controlled fashion at the beginning but after a certain instant it appears that it attains momentum and increases abruptly its thickness. The phenomenon is reminiscent of the bursting of the leading edge separation bubble. We intend to study such flows more carefully, with the electronic triggering equipment which we have now developed. A detailed description of the results will be included in the final version of the present report.

Experiments performed with smaller Reynolds numbers indicate a characteristically different behavior. Such experiments were performed

in the smaller facility, (Fig. 3.3) with glycerin and water mixtures in a ratio 60% by volume. The use of glycerin mixtures permits one to reduce the Reynolds numbers without simultaneous reduction of the velocities. It is therefore easier to observe the flow and capture a velocity field with a reasonable film exposure Δt. Examination of low Reynolds number flows using water as a testing medium would require very small velocities and unrealistically small Δt's. However, the use of glycerin has some distadvantages as well. The dimensionless number $L_i/L_p = (\nu/U^2 t)^{1/2}$ which describes the ratio of distances of diffusion propagation to particle displacement grows. As a result, the error involved when using the present method becomes larger. In the experiments performed with glycerin-water mixtures, L_d/L_p ranged between 0.05 and 0.12.

Transient flows were investigated again for low Reynolds numbers, that is the response of the flow to impulsive changes of the adverse pressure gradients. A more sophisticated triggering system is now being used. It involves a KIM-1 microprocessor (see Fig. 5.5) which is programmed to receive the signal of the initiation of the impulse and then activate the flash and trigger the camera at specified intervals of time. In this way it is possible to receive snapshots of the same phenomenon at different times and thus capture the evolution of one single unsteady flow field. In Fig. 5.6 we show a sequence of velocity fields taken with a camera speed of 1/2 sec. and a Reynolds number equal to 1000. The first frame represents the steady flow for $\theta = 0$. The second frame is shot with a delay $\Delta t_o = 0.5$ sec after an impulsive change of the flap angle from $\theta = 0$ to $\theta = 40°$. The following frames were received at intervals of $\Delta t = 1$ sec. The speed of exposure was kept rather low in order to reveal the properties of slow moving flow at the bottom of the

laminar boundary layer and in the separated region. Immediately after the initiation of the impulsive change, the flow indicates a violent departure from the steady state configuration. Very soon, two distinct recirculating regions appear and a saddle point configuration is formed at approximately the station where steady separation occured. These flow patterns could be interpreted as reversed flow upstream of separation, if separation were to be defined as the saddle point that is shown in this figure. The velocity fields shown in these frames are indeed fully contained in the viscous region of the flow. This becomes clear from velocity profiles derived from the visualization of Fig. 5.6 and shown in Fig. 5.7. However the first bubble seems to retain its identity even after the flow has arrived at its steady state condition. It is therefore possible that such recirculating bubbles are part of the wake which for low Reynolds numbers, is usually made up of a few discrete vortices. It should be emphasized that with larger viscosities, viscous diffusion is increased and the response of viscous phenomena, including separation, is faster. The sequence of photographs shown in Fig. 5.6 could be interpreted therefore as follows. Separation immediately moves upstream. The rearrangement of the vortices in time represents the familiar unsteadiness contained in the wake. This would be the interpretation that the numerical analyst would probably offer (Mehta and Lavan, 1975; Mehta, 1977). Indeed for low Reynolds numbers reversing of the flow direction could be defined as separation.

In Fig. 5.8 we show a sequence of velocity fields again for $R_e \tilde{=} 1000$ but with a final flap inclination $\theta_{II} = 30°$. The general characteristics of the flow are similar. In fact it is now easier to accept that the

leading recirculating bubble is part of the attached boundary layer. This sequence of experiments unfortunately does not help us to give the correct interpretation to the phenomenon. It appears quite possible and in fact our experimental data seem to support the idea, that with growing Reynolds numbers, the flow patterns shown in Figs. 5.6 and 5.8 are conserved but their dimension perpendicular to the wall shrinks together with the laminar boundary layer.

6. Separation Over a Fixed Surface With Outer Flow Accelerations

In another set of experiments and always for $R_e \approx 1000$, we studied the response of laminar separation to accelerating and decelerating outer flows. In these experiments the disturbing flap was completely removed and unsteadiness was introduced only via the change of the magnitude of the outer flow. It should be noted here that potential flow is unaffected by such changes and the streamline configuration of inviscid flow should remain undisturbed. The flow is governed by Laplace's equation

$$\nabla^2 \phi = 0 \tag{6.1}$$

with ϕ the potential function and time is introduced via the boundary conditions, in this case the free stream velocity. However, in inviscid flow the pressure is given by Bernoulli's equation

$$\frac{\partial \phi}{\partial t} + \frac{V^2}{2} + \int \frac{dp}{\rho} = f(t) \tag{6.2}$$

where V, p and f(t) are the velocity pressure and an arbitrary function of time respectively. Clearly time variations of ϕ generate pressure disturbances which in turn influence to location of separation.

In Fig. 6.1 we show a sequence of velocity profiles for a flow accelerating from U_∞ = 12 cm/sec to U_∞ = 25 cm/sec. The visualization at t = 0 corresponds to the undisturbed flow. The flow at intervals Δt_o = 0.5 and Δt = 1 sec after the initiation of the acceleration is shown in the same figure. An inspection of the outer flow is enough to convince that during the acceleration process the outer flow essentially

"washes away" the separated region. Indeed separation is displaced downstream and eventually moves out of the frame of observation. Subsequently and after the outer flow has achieved the new steady velocity of 25 cm/sec, the point of separation slowly moves again into the picture and arrives at almost its initial position. This was expected since for $R_e \simeq 1000$ or above, the location of separation in steady flow is insensitive to the magnitude of the outer flow velocity.

Velocity profiles received from these visualizations are shown in Fig. 6.2. These profiles correspond to the stations A and B, that is, the point above the scale marker and 60 mm upstream, as shown in Fig. 5.1. The flow at point A is probably a very small distance downstream of the point of steady separation. The velocity profile at this point clearly shows a vanishing of the skin friction, or perhaps a small region of slow reversed flow. After the acceleration of the outer flow begins, the wall shear becomes positive and increases sharply. The inflection point of the profile disappears and only after the outer flow achieves its final value, we observe a sharp decrease of the velocity profile and the appearance of a point of inflection and a vanishing value of the velocity at the same distance from the wall as for $t < 0$. Normalized velocity profiles are shown in Fig. 6.3.

A sequency of instantaneous velocity fields for decelerating flows is shown in Fig. 6.4. In this case the point of separation is displaced sharply upstream, while the separated region thickens sharply. As time grows the flow pattern returns again to its original configuration.

A plot of the excursions of separation for accelerating and decelerating flows is shown in Fig. 6.5. In the same figure we show the variations of the outer flow for comparison. It appears that the time scale of the

response of separation is of the same order of magnitude with the scale of changes of the outer flow. Experiments repeated with much smaller accelerations resulted in weaker displacements of the point of separation, until no effect at all could be observed.

Conclusions

As mentioned earlier, this is only a preliminary report based on the information received until the end of November 1977. A lot of time on this project was devoted to the construction and calibration of the facilities and the perfection of the experimental methods developed. As a result, meaningful experimental data on unsteady separation did not become available until the middle of 1977. Work is being continued and experimental data is now received without interruptions.

The data presented in the present report and the ones being presently received, should be revaluated. Some new information on the properties of unsteady separation is already contained in the present report. However, it is felt that the information is somewhat fragmented. The Sears model for unsteady separation, that is the criterion $u = \partial u/\partial y = 0$ in a frame of reference moving with separation, will be tested against the experimental results, whenever possible. During the process of interpretation and documentation of the experimental results, it is always kept in mind that numerical analysis may have to follow. Provisions are therefore taken to simplify the geometrical configurations and supply all the necessary information on the boundary and initial conditions.

References

Carr, L. W., McAlister, K. W. and McCroskey, W., 1977, "Analysis of the Development of Dynamic Stall Based on Oscillating Airfoil Experiments", NASA TN D-8382.

Fage, A. 1934, Proc. Royal Soc. A 144, 381.

Fansler, K. S. and Danberg, J. E. 1976 "Boundary-Layer Development on Moving Walls Using an Integral Theory", AIAA J. 14, 1137.

Homann, F. 1937 Forsch. Geb. Ing. Wes., 7, 1.

Ludwig, G. R., 1964 "An Experimental Investigation of Laminar Separation from a Moving Wall", AIAA Paper 64-6.

McCroskey, J. J., 1971, "Dynamic Stall on a Helicopter Rotor Blade," Proceedings of SQUID Workshop, Atlanta, ed., Marshall, F. J., pp. 346-350.

Mehta, U. B. and Lavan, Z, 1975, "Starting Vortex, Separation Bubbles and Stall-a Numerical Study of Laminar Unsteady Flow around an Airfoil, J. Fluid Mechanics, 67, 227-256.

Mehta, U. B., 1977, "Dynamic Stall of an Oscillating Airfoil, in Unsteady Aerodynamics, Proceedings of an AGARD Symposium, Paper No. 23.

Moore, F. K. 1958, "On the separation of the Unsteady Boundary Layer", Boundary Layer Research. H. Gortler, ed. Springer, Berlin, 296.

Prandtl, L., 1904, "Uber Flussigkeitsbewegung bei sehr kleiner Reibung", Proc. Intern. Math. Congr. Heidelberg, 484-91.

Pruppacher, H. R., LeClair, B. P. and Hamielec, A. E., 1970, "Some Relations Between Drag and Flow Pattern of Viscous Flow past a Sphere and a Cylinder at Low and Intermediate Reynolds Numbers", J. Fluid Mech., 44, 781-790.

Rott, N., 1956, Unsteady Viscous Flow in the Vicinity of a Stagnation point. Quart. Appl. Math. 13, p. 444.

Rott, N., 1964, Theory of time dependent laminar flows, in Theory of Laminar Flows, F. K. Moore (ed.), Princeton University Press, Princeton, N.J.

Ruiter, G. H., Nagib, H. M., and Fejer, A. A., 1971, "Unsteady Boundary-Layer Separation over Oscillating Airfoils," Proceedings of SQUID Workshop, Atlanta, ed., Marshall, F. J., pp. 423-425.

Sandborn, V. A. and Liu, C. Y., 1968, "On Turbulent Boundary-Layer Separation", J. Fluid Mech., 32, 293-304.

Schraub, F. A., Kline, S. J., Henry, J., Rumstadler, P. W., and Littel, A., 1965, "Use of Hydrogen Bubbles for Quantitative Determination of Time Dependent Velocity Fields in Low-Speed Water Flows", J. of Basic Eng., 87, 429-444.

Sears, W. R., 1956, "Some Recent Developments in Airfoil Theory", J. Aero. Sciences, 23, 490-499.

Sears, W. R. and Telionis, D. P., 1975, "Boundary Layer-Separation in unsteady flow", S.I.A.M. J. of Appl. Math. 28, 215.

Taneda, S., J. Phys. Soc. Japan, 11, 302.

Telionis, D. P., 1970, "Boundary Layer Separation", Ph.D. Thesis, Cornell University, Ithaca, N.Y.

Telionis, D. P., 1976, "Critical Points and Streamlines in Viscous Flows", Virginia Polytechnic Institute and State University, Engineering Report, No. VPI-E-76-28.

Telionis, D. P., 1977, "Unsteady Boundary Layers-Attached and Separated", in Unsteady Aerodynamics, Proceedings of an AGARD Symposium, Paper No. 17.

Telionis, D. P., and Werle, J., 1973, "Boundary-Layer Separation from Downstream Moving Boundaries", Journal of Applied Mechanics, 95, 389-374.

J. S. Tennant, 1973, "A Subsonic Diffuser with Moving Walls for Boundary-Layer Control", AIAA J. 11, 240-242.

Tennant, J. S. and Yang, T., 1973, "Turbulent Boundary-Layer Flow from Stationary to Moving Surfaces" AIAA J., 11, 1156-1160.

Tsahalis, D. TH., 1977, Laminar Boundary Layer Separation from an Upstream Moving Wall, AIAA J., 15, 561-566.

Vidal, J. R., 1959, "Research on Rotating Stall in Axial-Flow Compressors, Part III", WADC TR-59-75.

Williams, III, J. C., 1977, Incompressible Boundary-Layer Separation, in Annual Review of Fluid Mechanics, Annual Reviews Inc., 9, 113-144.

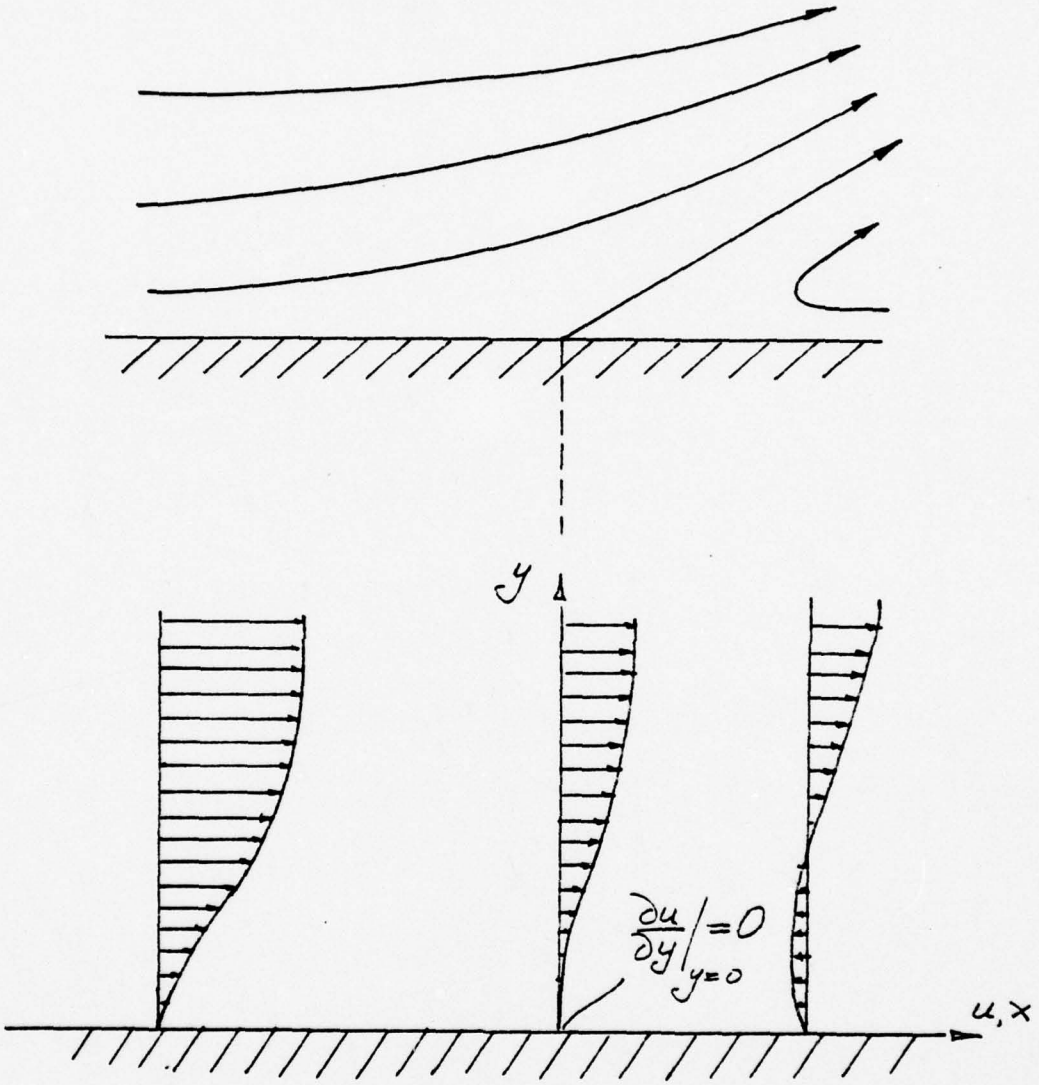

Fig. 1.1 Separation over a fixed wall

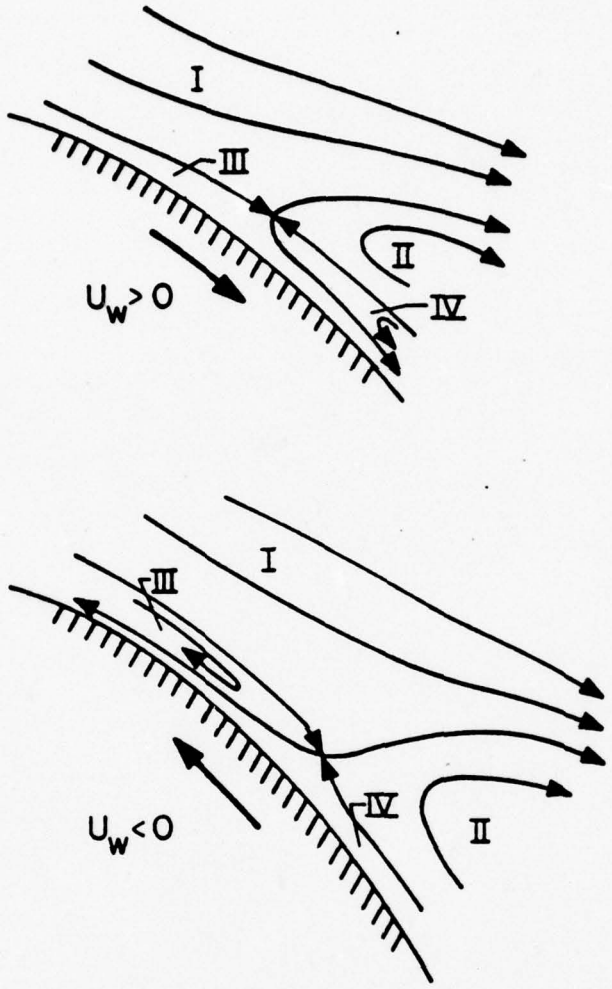

Fig. 1.2 Separation over moving walls

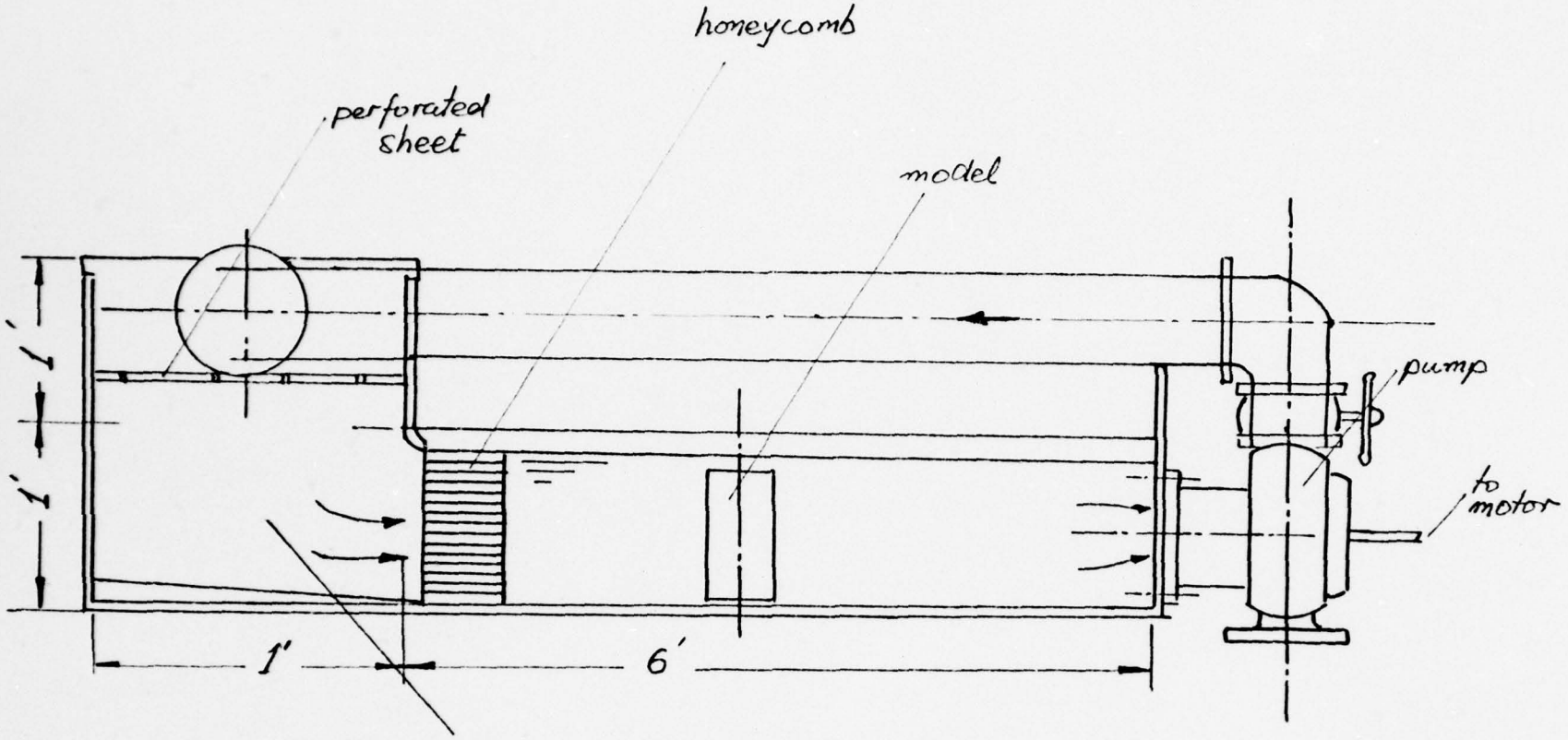

Fig. 2.1 The open recirculating tank

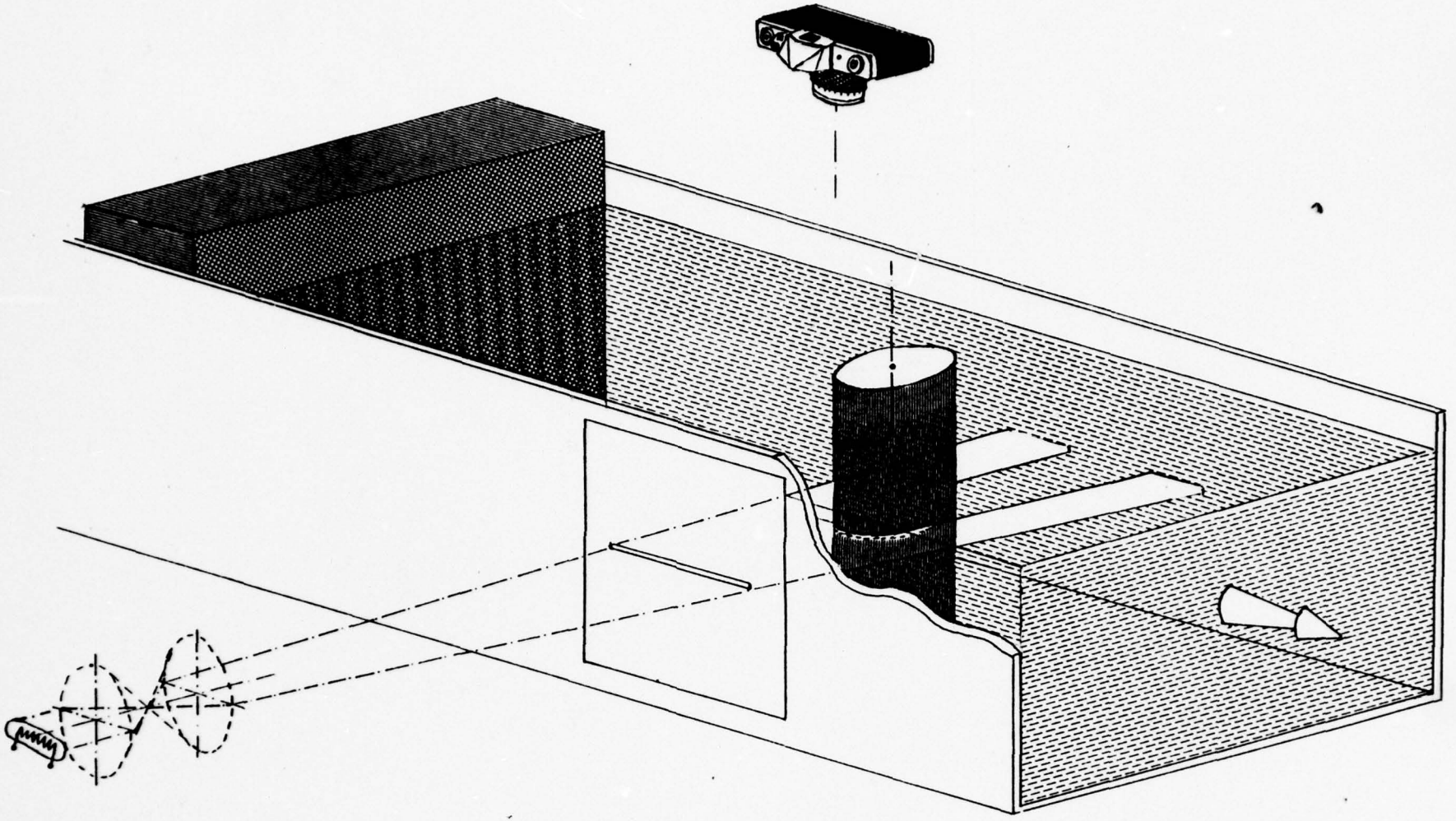

Fig. 2.2 Schematic representation of the optical arrangement and the test section

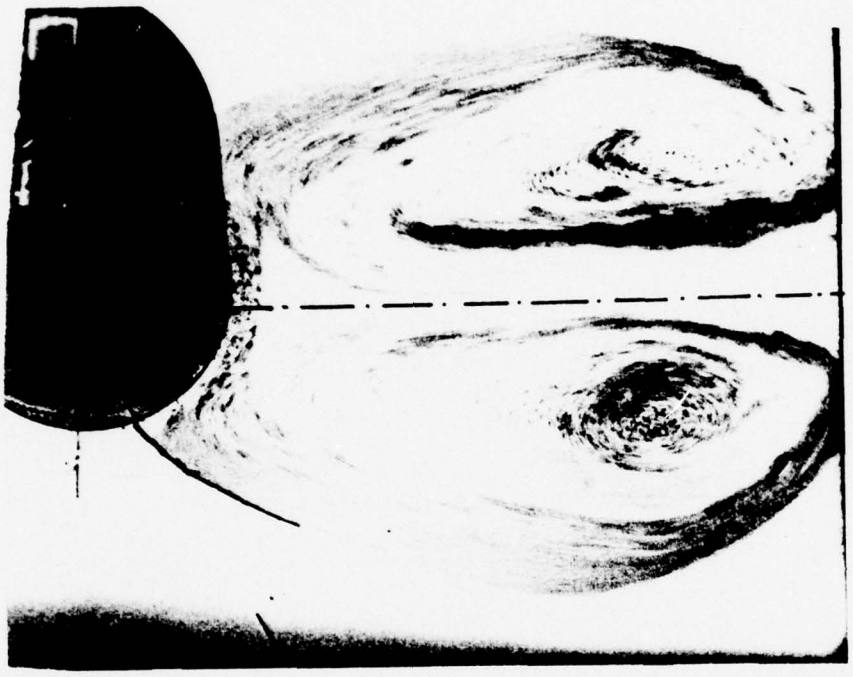

Fig. 2.3 The wake of a circular cylinder for $R_e = 40$

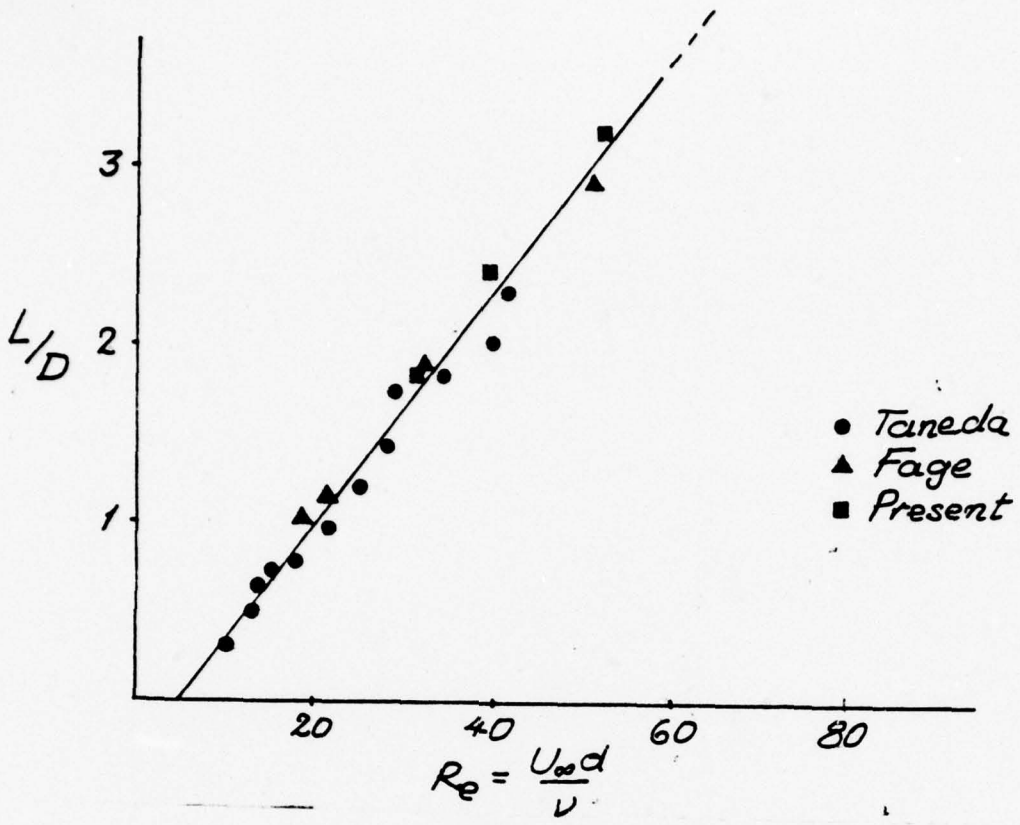

Fig. 2.4 The length of the wake as a function of the reynolds number

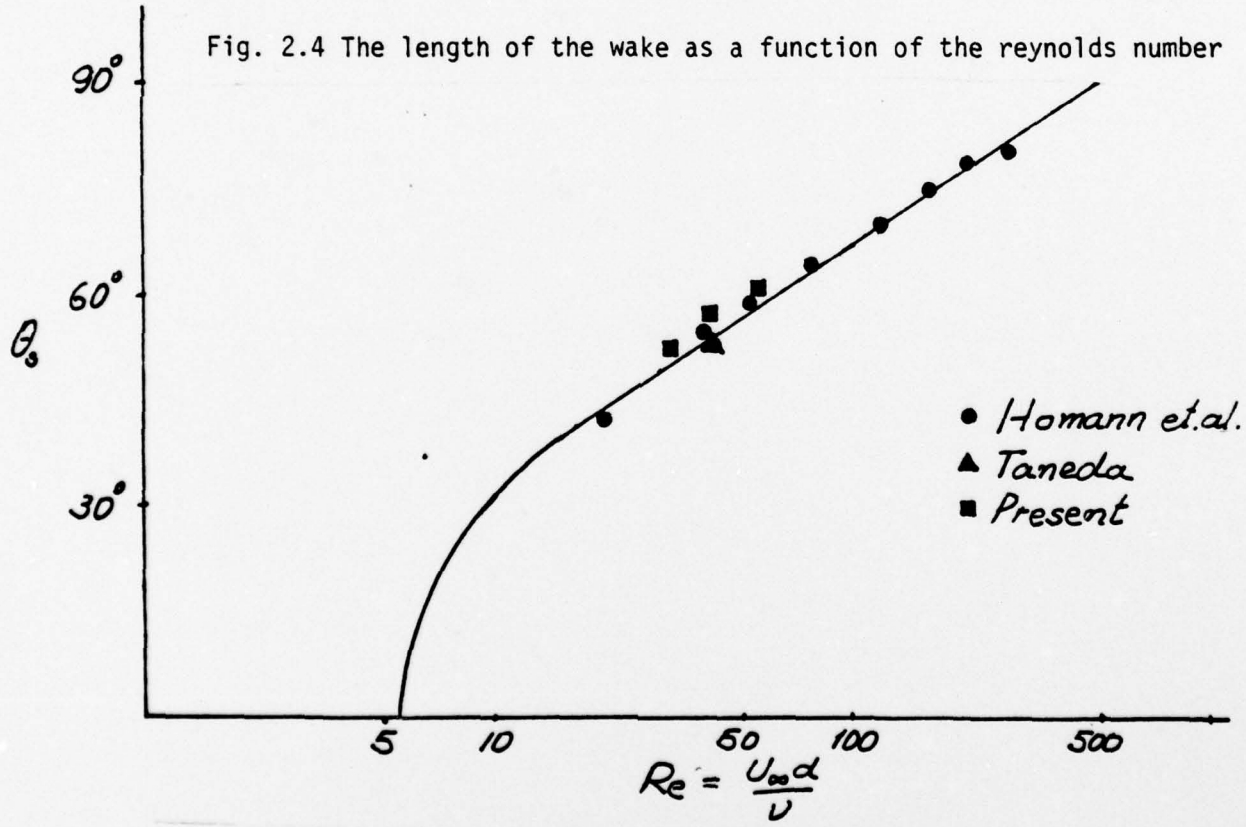

Fig. 2.5 The angle to separation as a function of the reynolds number

Fig. 2.6 Separation over a downstream moving wall for u_w/U_∞ =. and R_e = 50

Fig. 2.7 Separation over an upstream moving wall for u_w/U_∞ =1 and R_e = 50

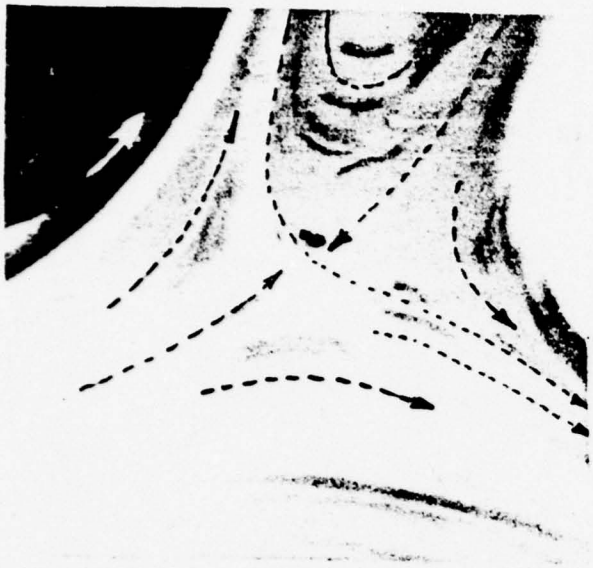

Fig. 2.8a Detail showing the saddle-point pattern for a downstream moving wall.

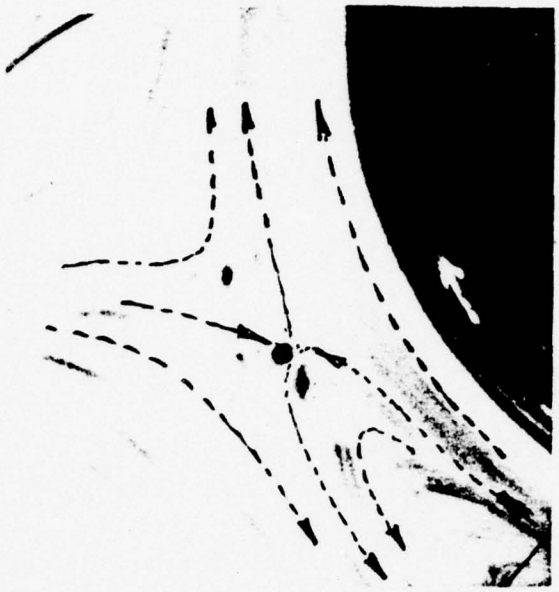

Fig. 2.9a Detail showing the saddle-point pattern for an upstream moving wall.

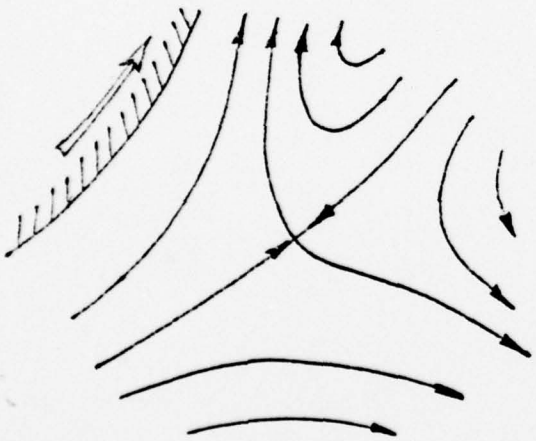

Fig. 2.8b Streamlines received from Fig. 2.8a

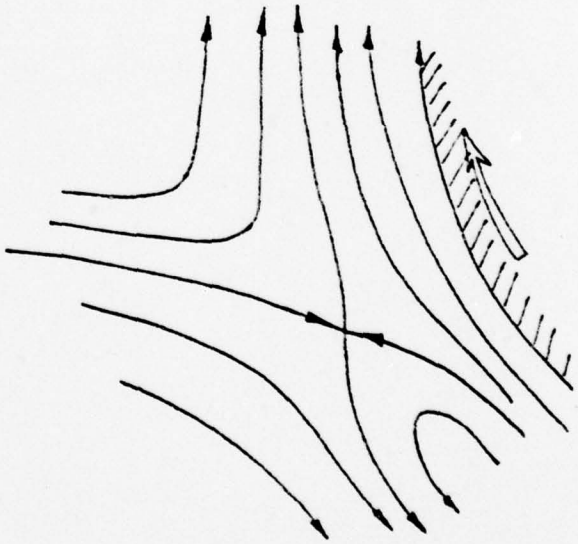

Fig. 2.9b Streamlines received from Fig. 2.9a

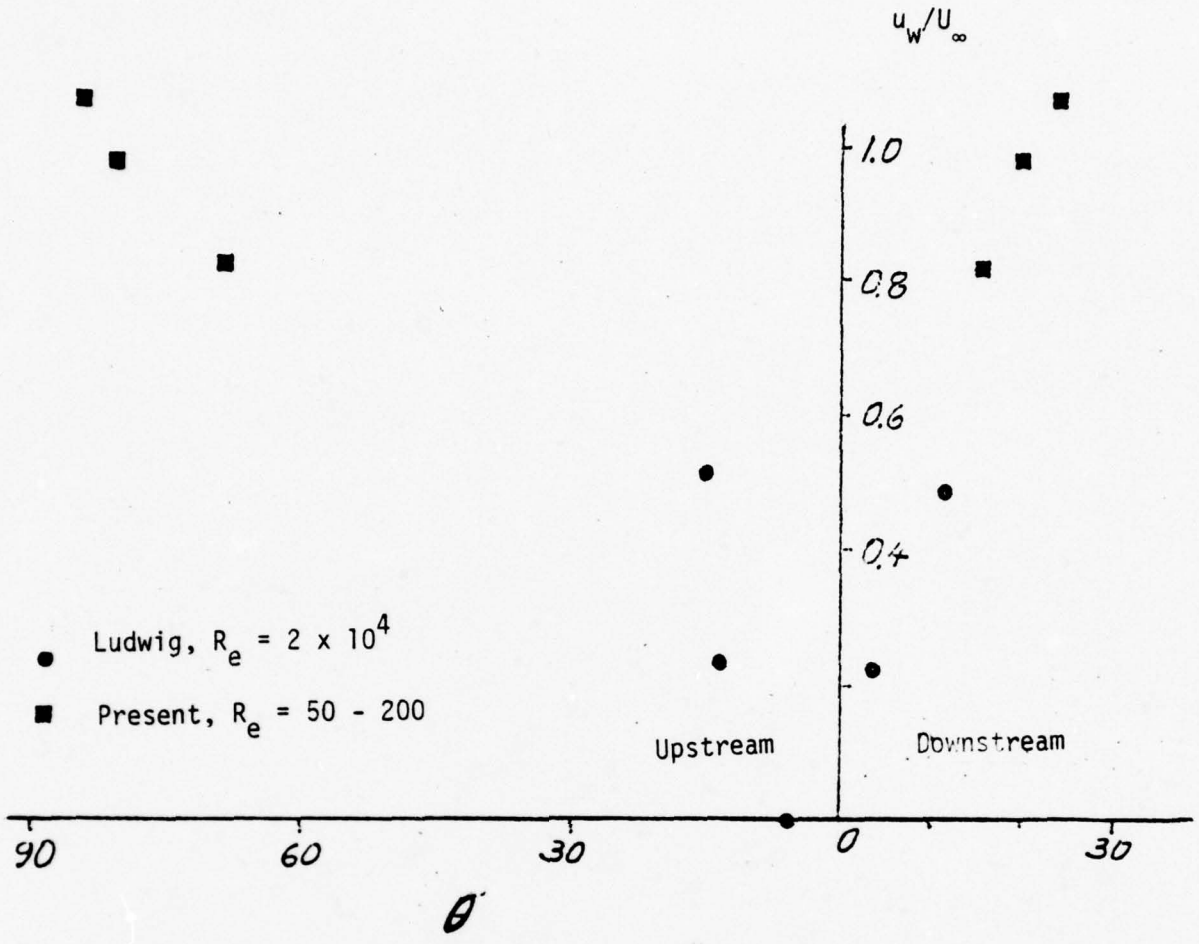

Fig. 2.10 Displacement of separation with the wall velocity ratio, u_w/U_∞.

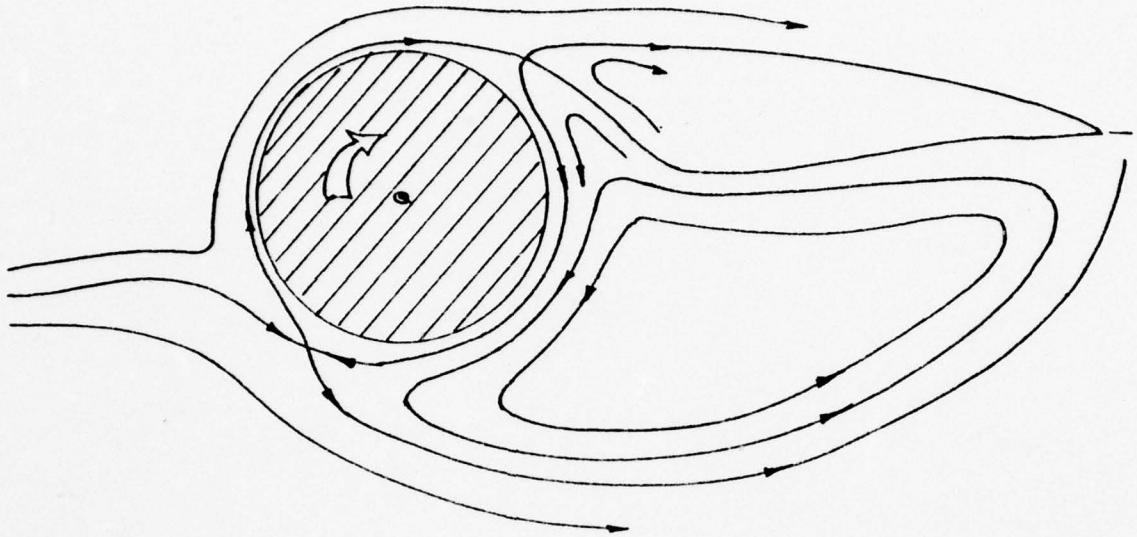

Fig. 2.11 Streamline pattern for low-Reynolds number flow over a circular cylinder.

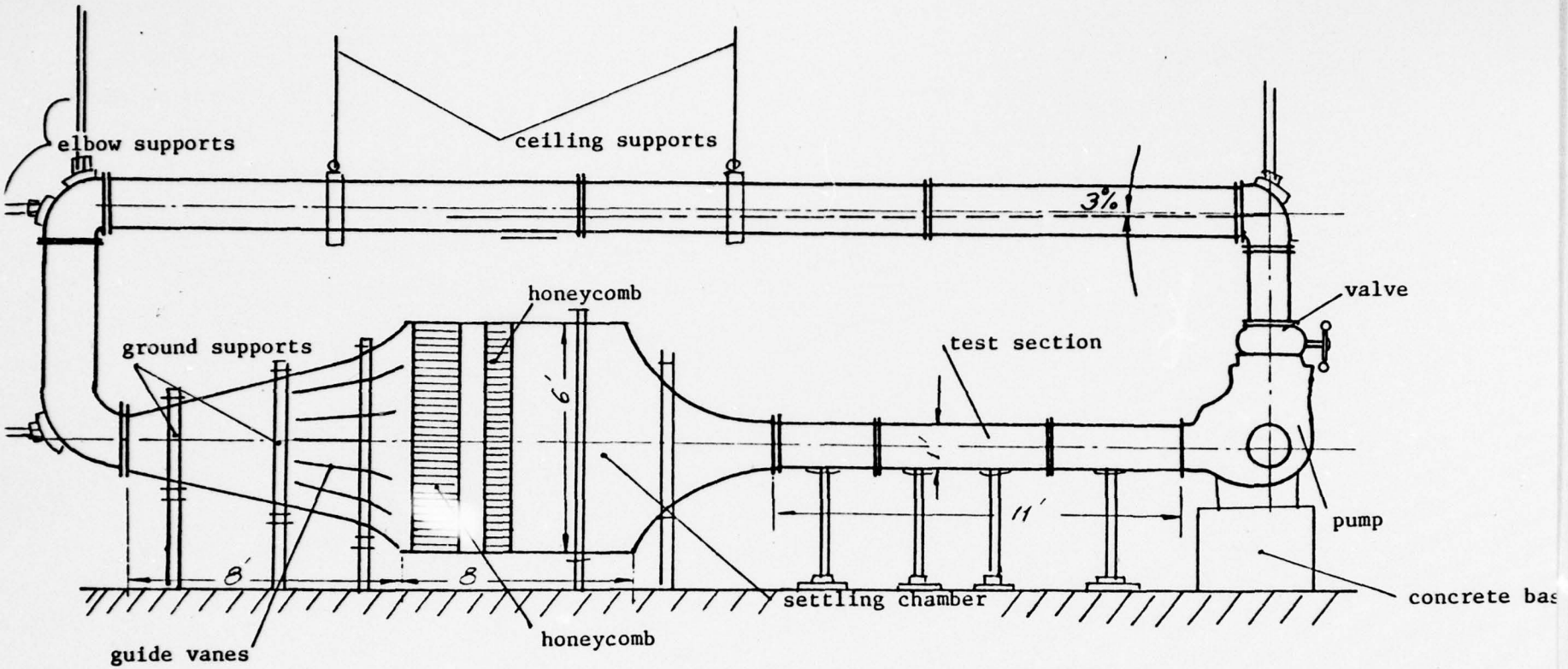

Fig. 3.1 The V.P.I. low speed water tunnel.

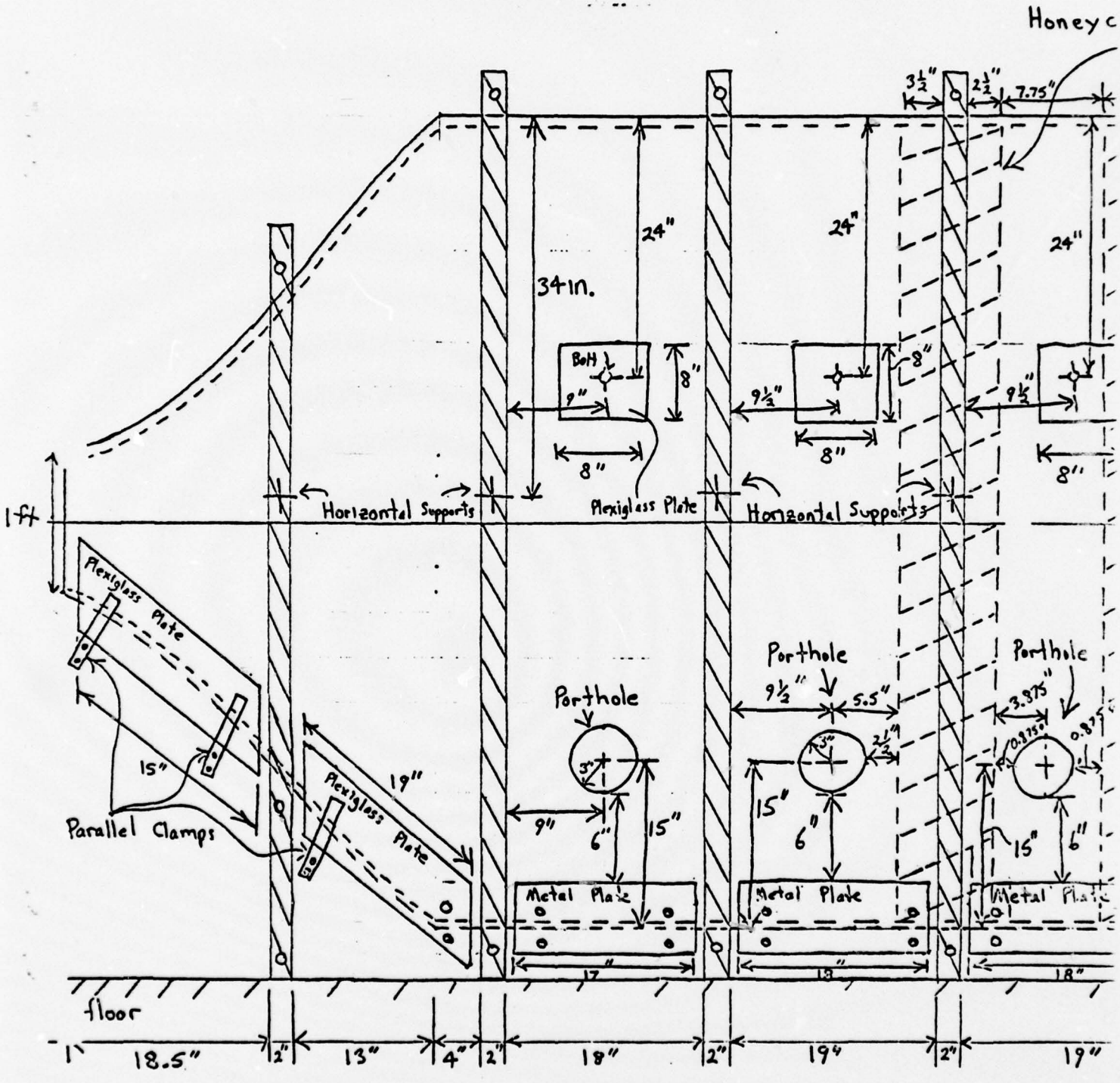

Fig. 3.2a Settling chamger, side view (left)

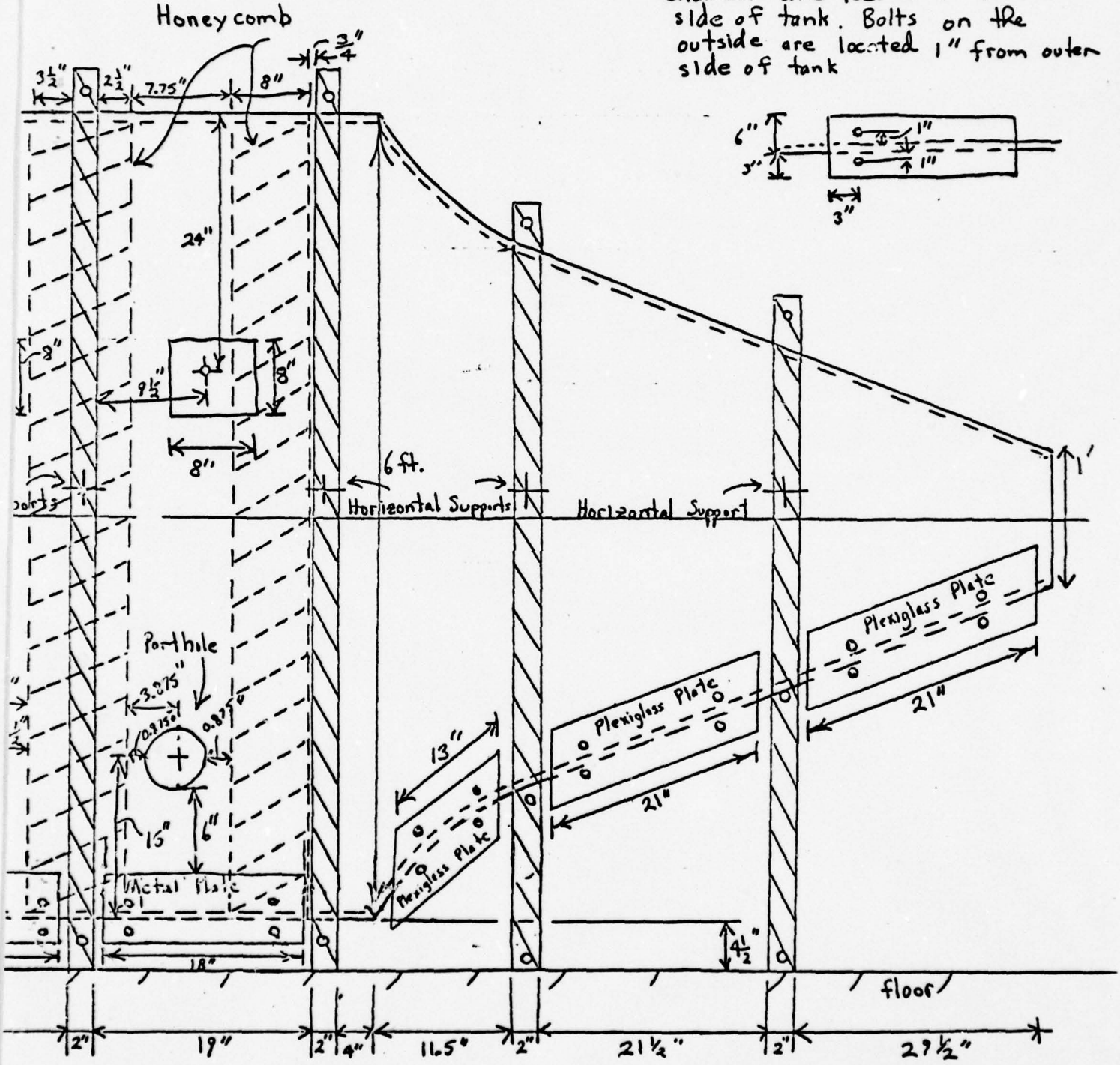

① Note: Bolts are located 3" from each end of plates. Plates are 9 in. wide, 6 in. on the tank and 3" overlap. Bolts inside the chamber are located 1" from inner side of tank. Bolts on the outside are located 1" from outer side of tank

Fig. 3.2b Settling chamber, side view (right)

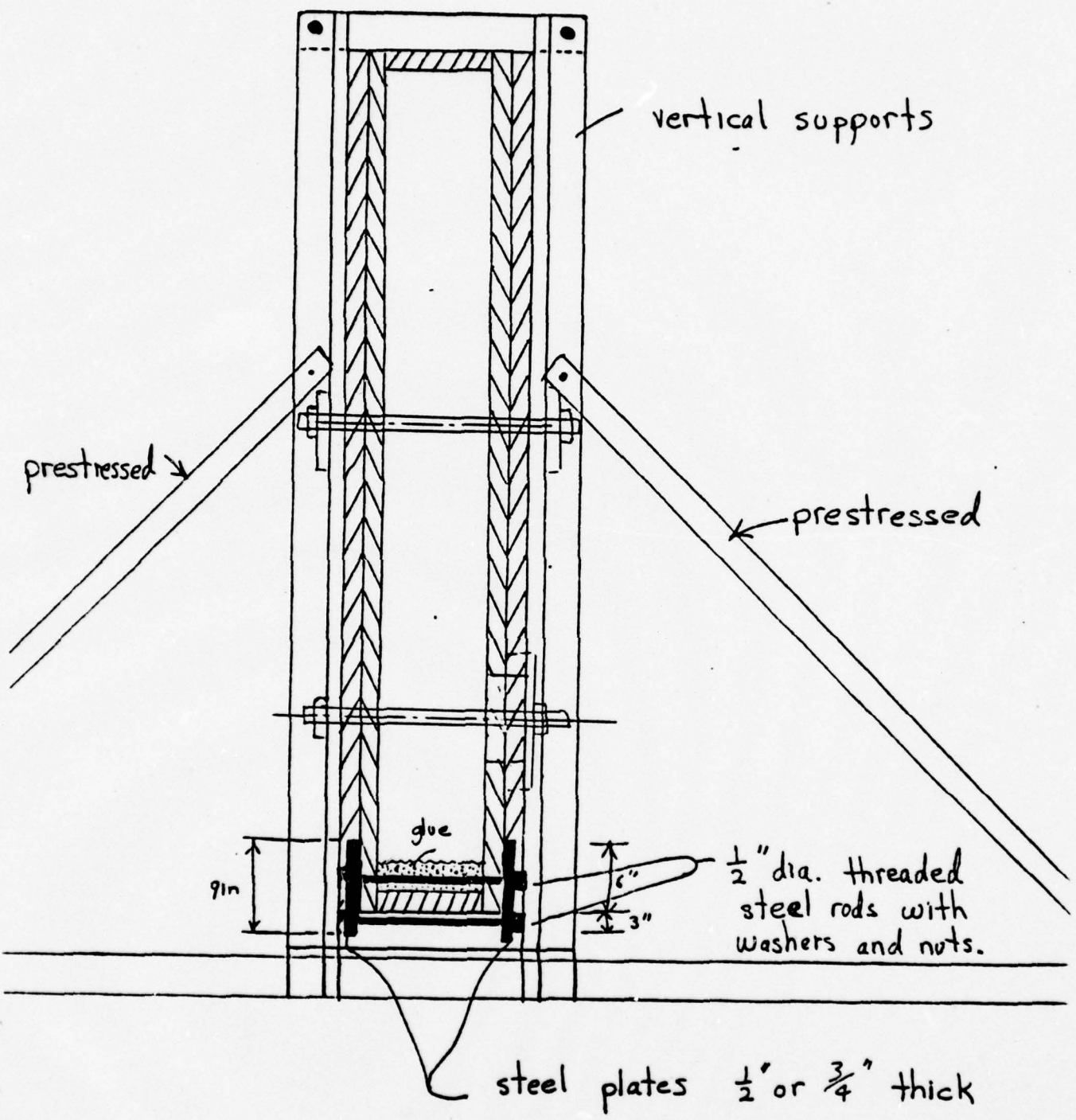

Fig. 3.2c Settling chamber, cross section

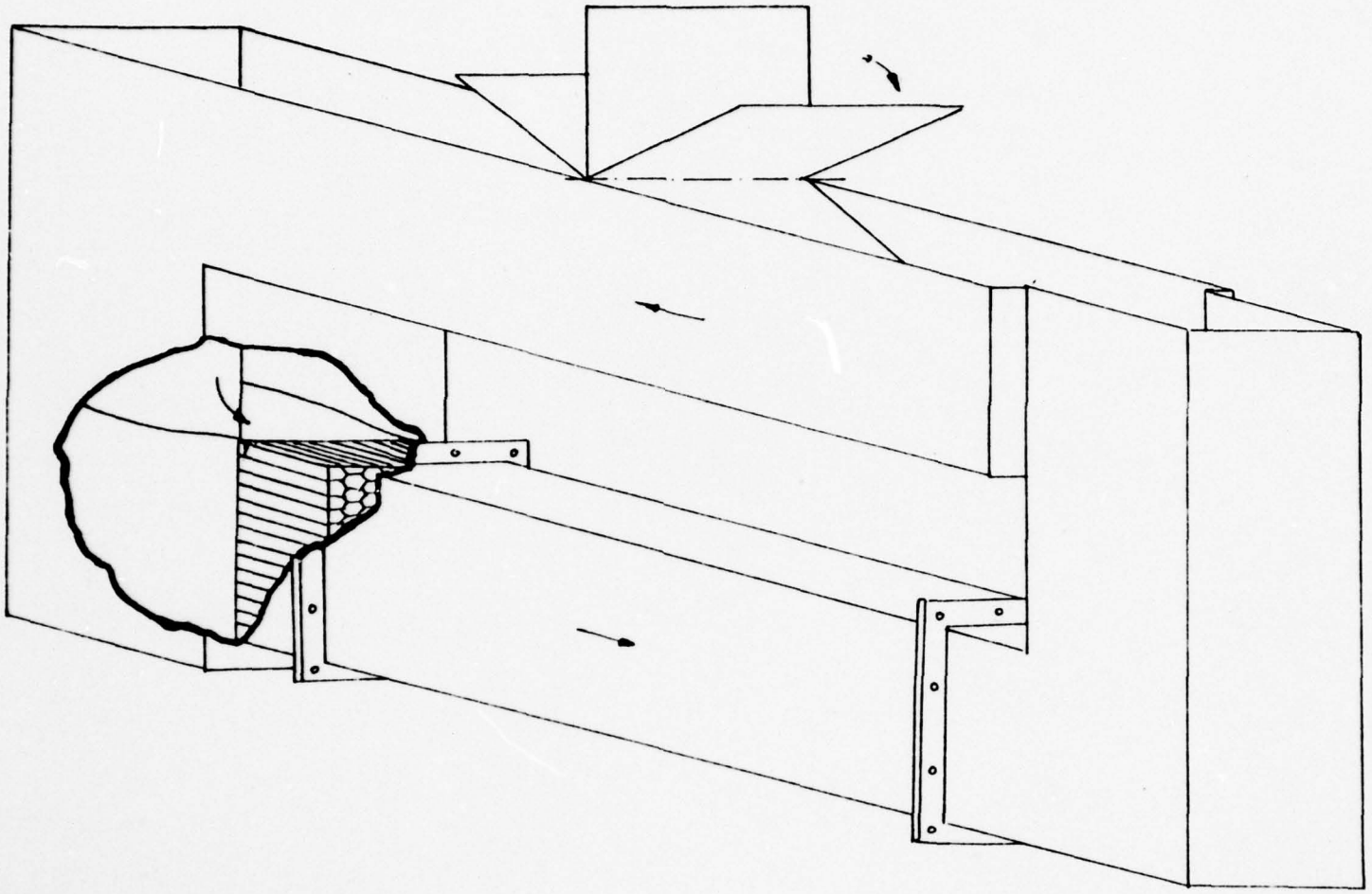

Fig. 3.3 The V.P.I. free-surface water tunnel

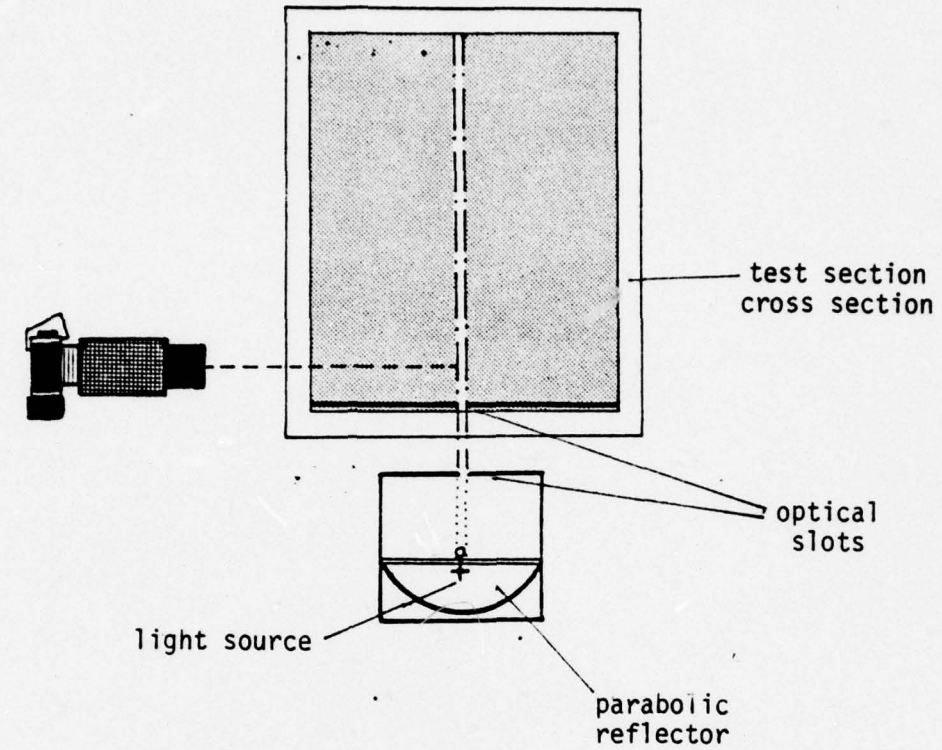

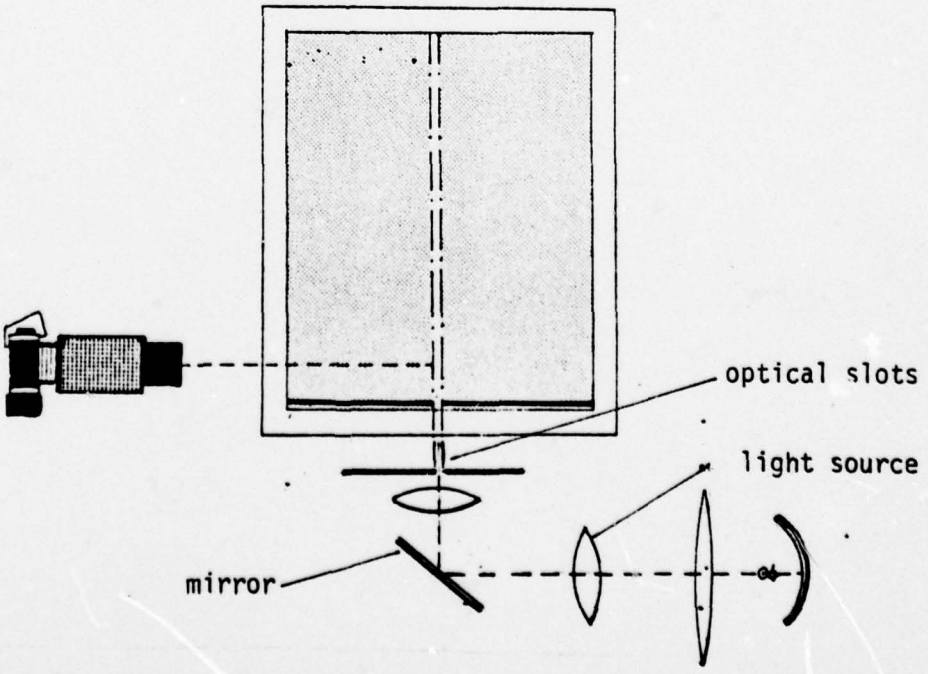

Fig. 4.1 The optical system for flow visualization.

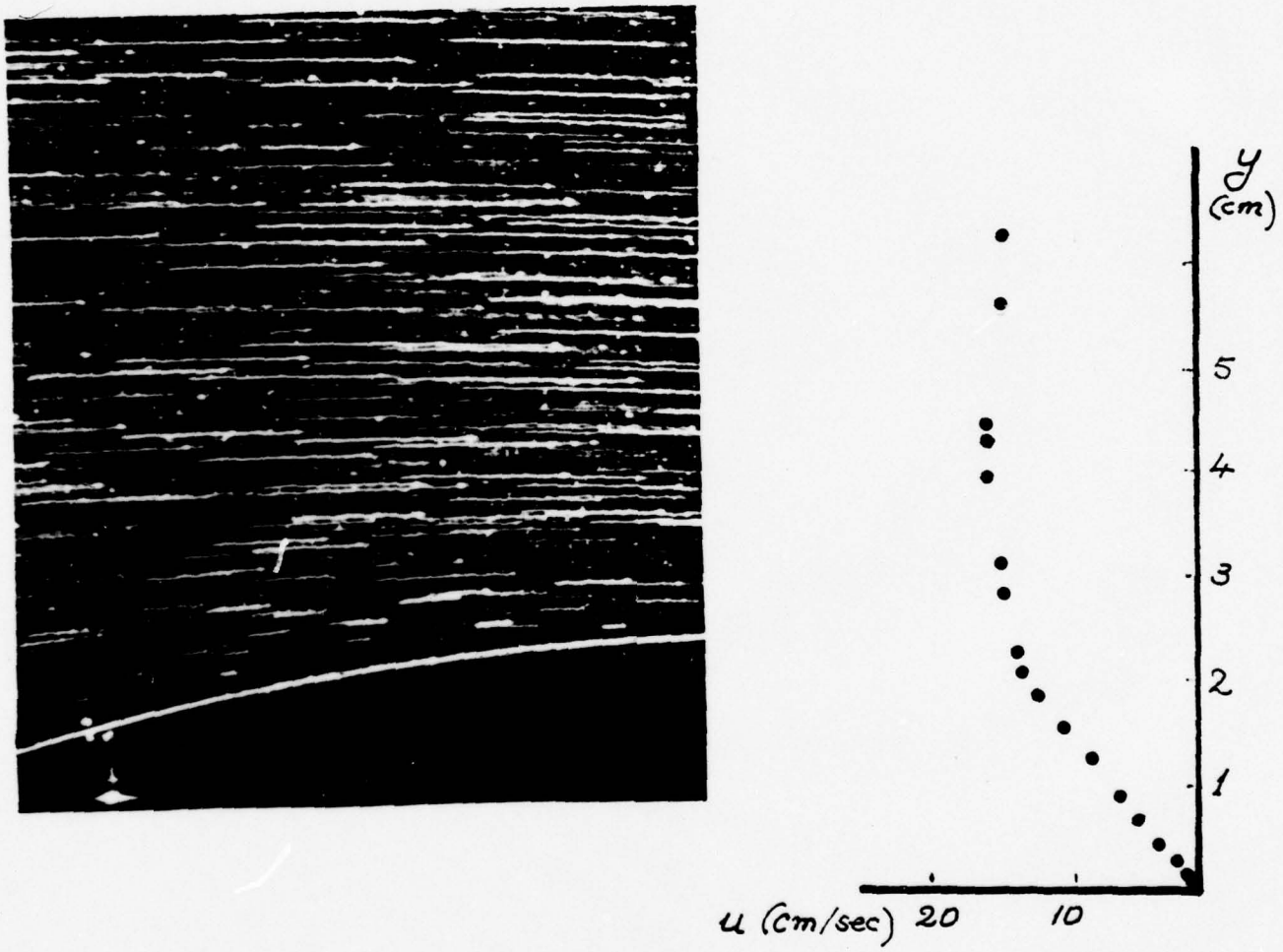

Fig. 4.2 Typical example of flow visualization showing the direction and magnitude of the velocity and a velocity profile at approximately the middle of the frame

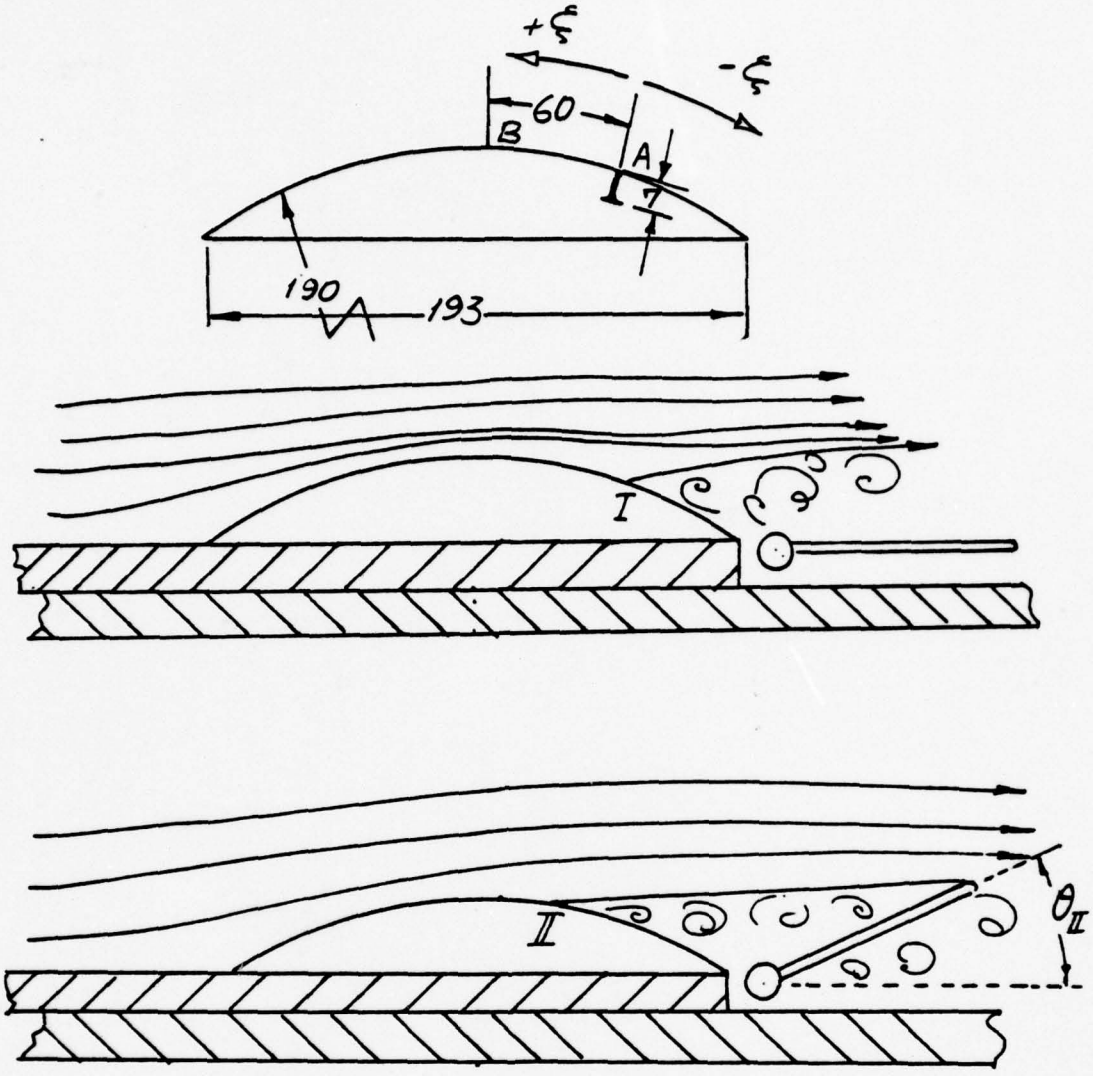

Fig. 5.1 The model used and the flap positions that induce separation. All the dimensions are in mm.

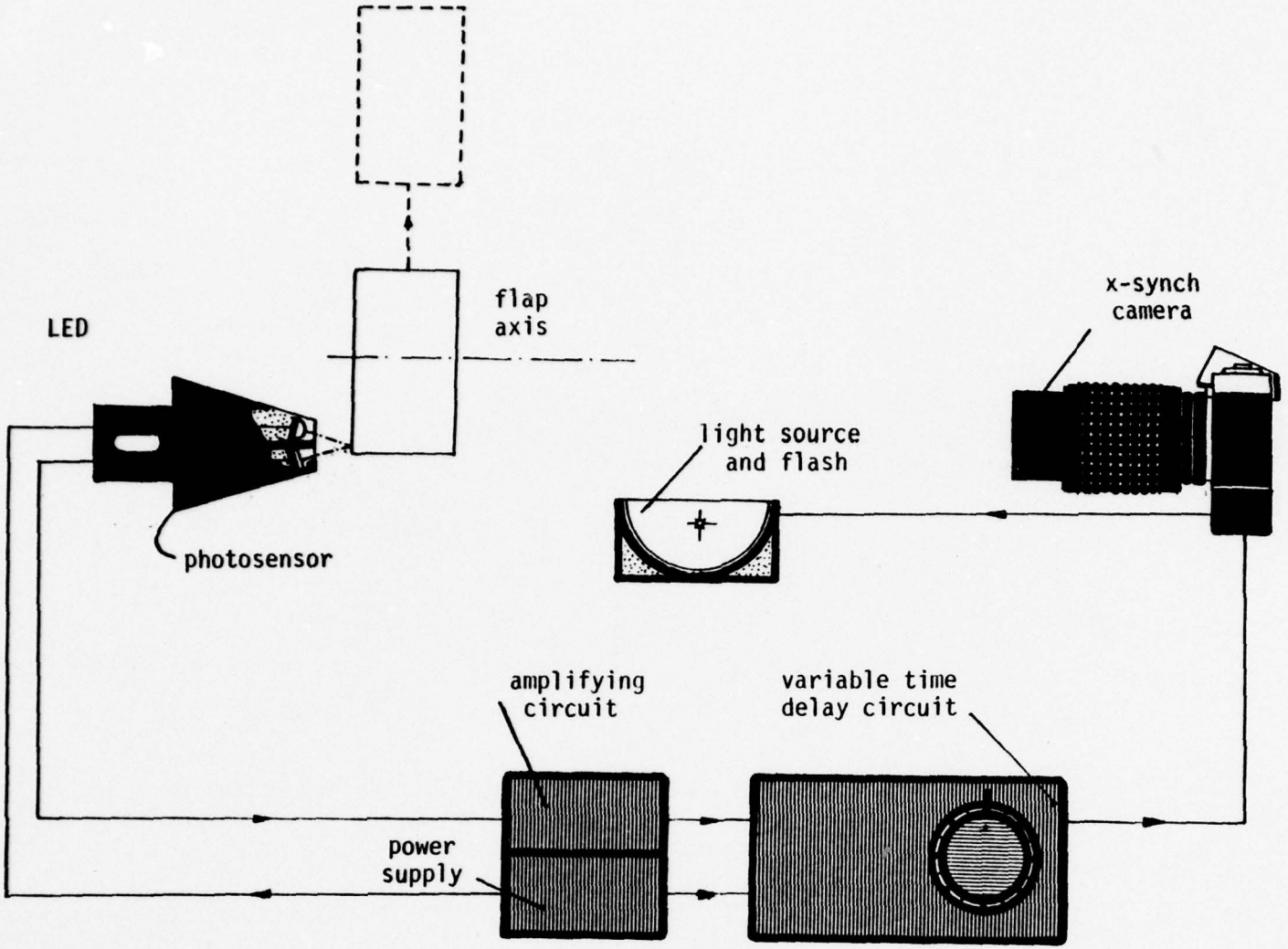

Fig. 5.2 Electronic circuit for triggering the disturbance generator and the camera.

Fig. 5.3 Flow visualization of an upstream moving separation with $R_e \sim 10^5$

Fig. 5.3 Flow visualization of an upstream moving separation with $R_e \sim 10^5$

t=0.2

t=0.5

Fig. 5.4 Dye visualization of the phenomenon depicted in Fig. 5.3.

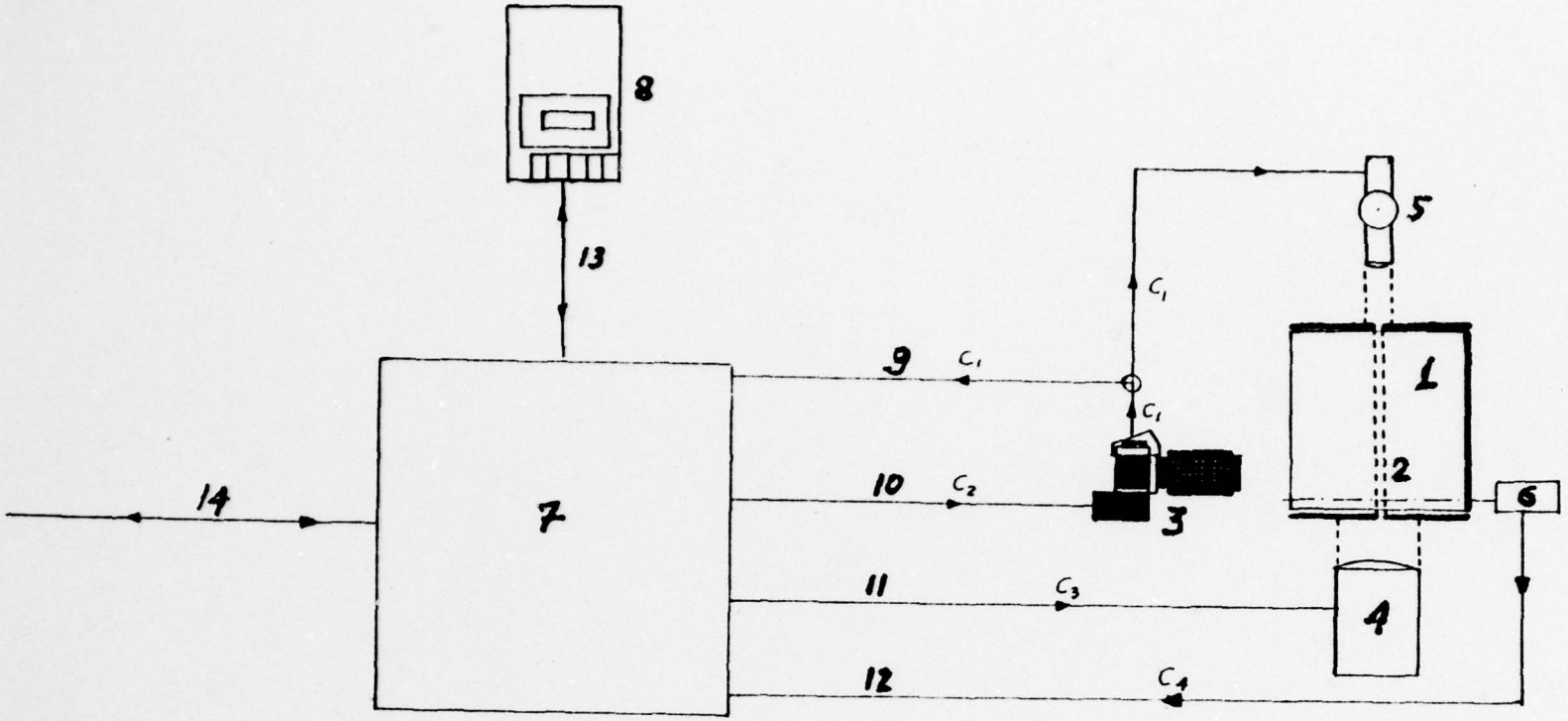

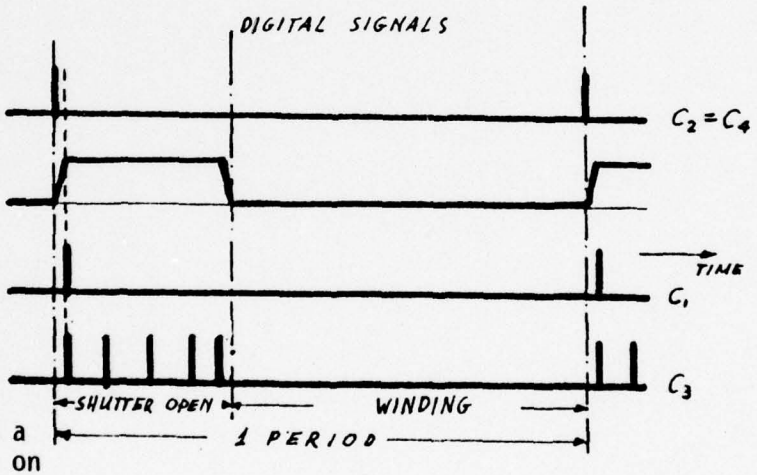

Fig. 5.5 The triggering system interfaced with a microprocessor. Complete description on the next page.

CAPTION TO 5.5

1. TEST SECTION WITH TRANSPARENT WALLS (CROSS SECTION)

2. PLANE OF LIGHT (OBSERVATION PLANE)

3. OLYMPUS OM-1 MOTOR DRIVE CAMERA (3 FRAMES PER SECOND) WITH VIVITAR 90mm f2.8 MACRO LENS(1:1 MAGNIFICATION RATIO)

4. FAST RECYCLING XENON STROBE(UP TO 20 FLASHES PER SECOND) COMBINED WITH CONTINUOUS OUTPUT 1000W QUARTZ LAMP IN THE SAME HOUSING AND FOCUSED AT INFINITY BY A LENS

5. VIVITAR 283 STROBE (UP TO 3 FLASHES PER SECOND) FOCUSED AT INFINITY BY A LENS

6. OSCILLATOR (VARIABLE SPEED MOTOR OSCILLATING A SHAFT)

7. KIM-1 (MOS) MICROPROCESSOR (6502 ARRAY) WITH TWO 6530 ARRAYS (ROMS), 1152 BYTES OF "READ" "WRITE" MEMORY, TWO PROGRAMMABLE INTERVAL TIMERS, SIX LED DISPLAY, KEYBOARD, AUDIO CASSETTE INTERFACE, TTY INTERFACE

8. AUDIO CASSETTE RECORDER INTERFACED WITH THE MICROPROCESSOR

9. CAMERA'S SHUTTER OPEN FEEDBACK THROUGH CAMERAS X SYNCH AND SLOW STROBE'S (5) CONTROL LINE

10. MOTOR DRIVE CONTROL LINE

11. FAST STROBE'S (4) CONTROL LINE

12. R.P.M. 2 PHASE FEEDBACK THROUGH A LED/PHOTOSENSOR

13. AUDIO CASSETTE INTERFACE

14. TTY INTERFACE WITH IBM COMPUTER (OPTIONAL)

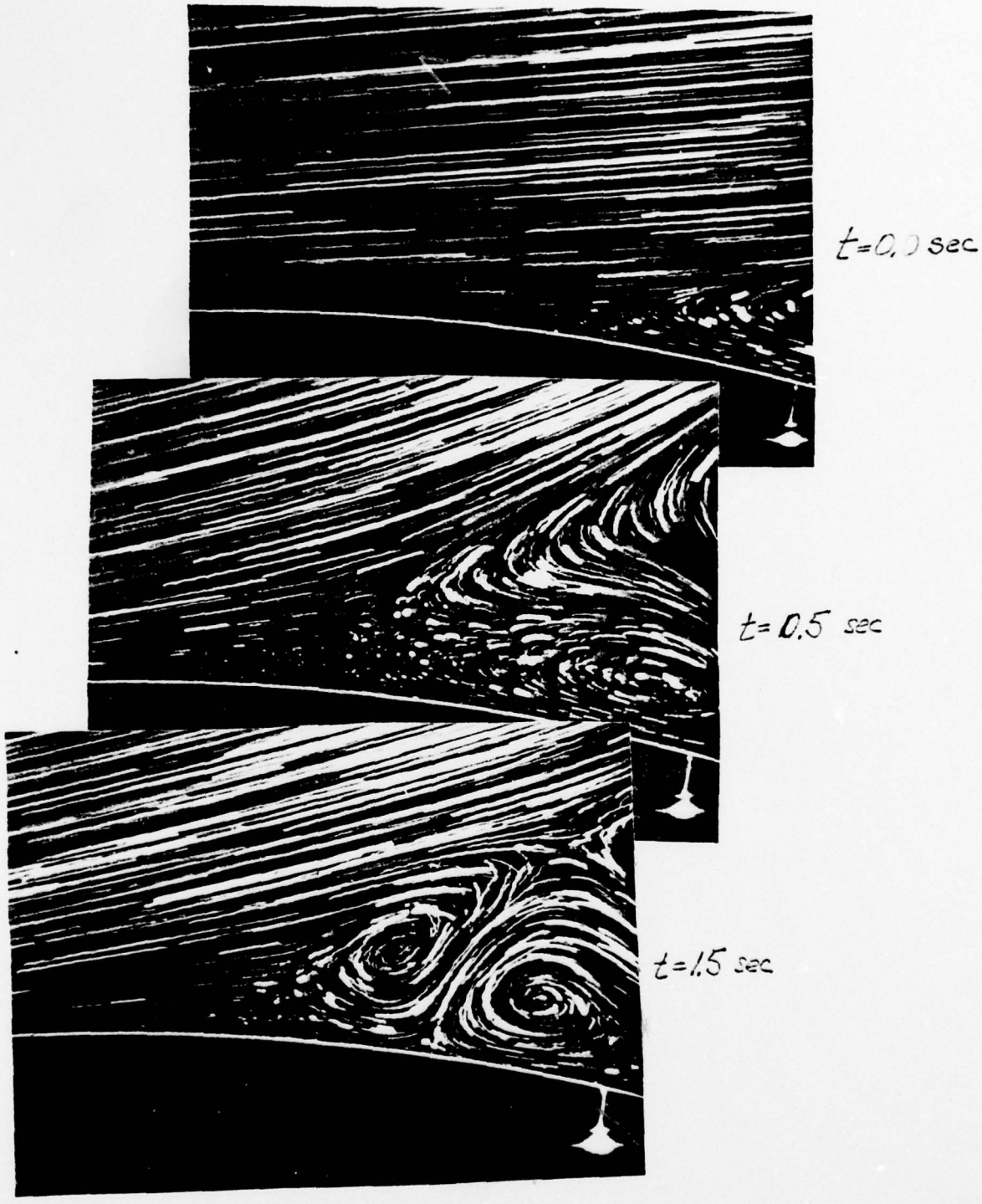

Fig. 5.6 Flow visualization of instantaneous velocity fields for an impulsive change $\theta_I = 0$ to $\theta_{II} = 40°$ and $R_e \cong 1000$

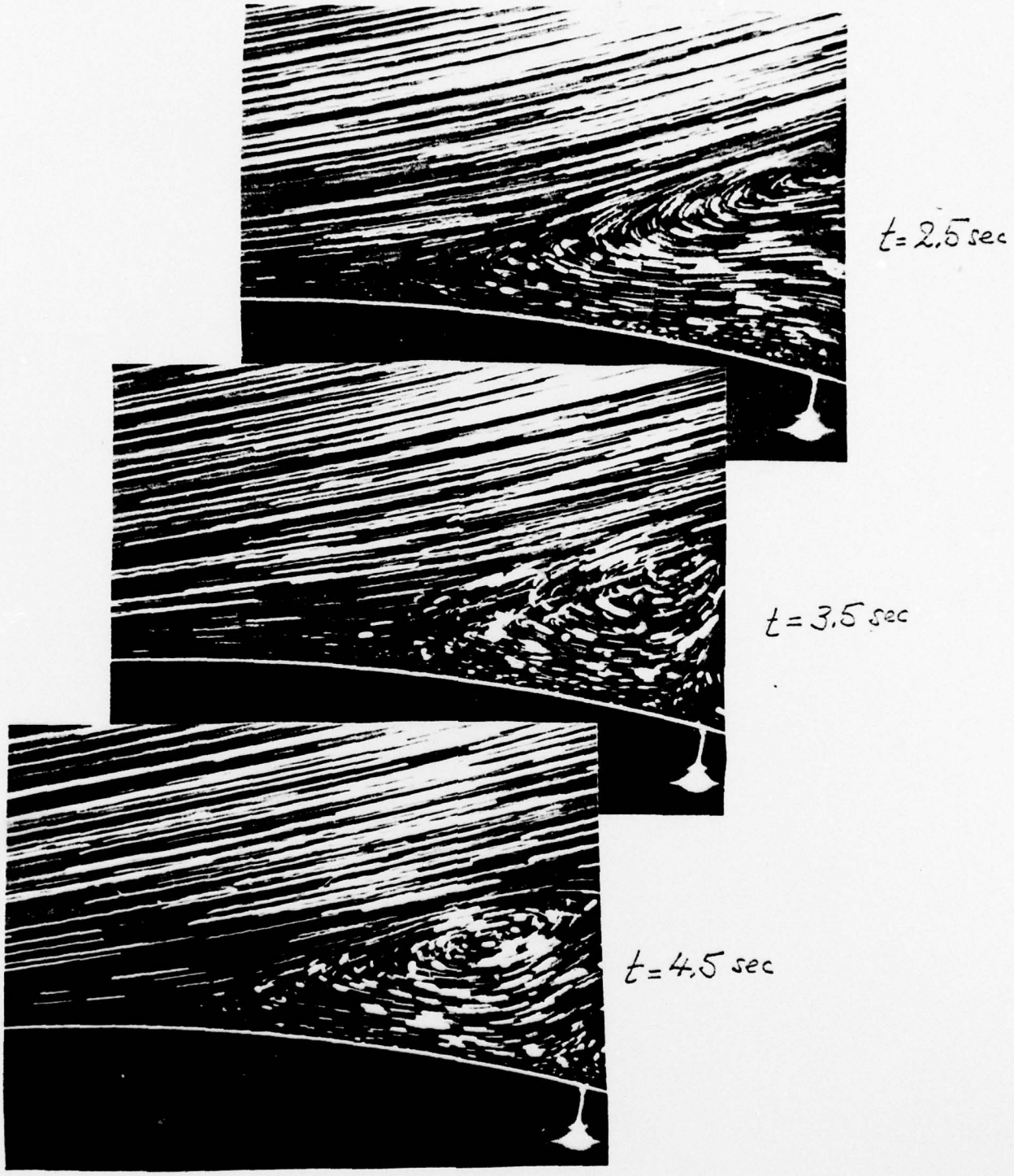

Fig. 5.6 (continued) Flow visualization of instantaneous velocity fields for an impulsive change $\theta_I = 0$ to $\theta_{II} = 40°$ and $R_e \cong 1000$

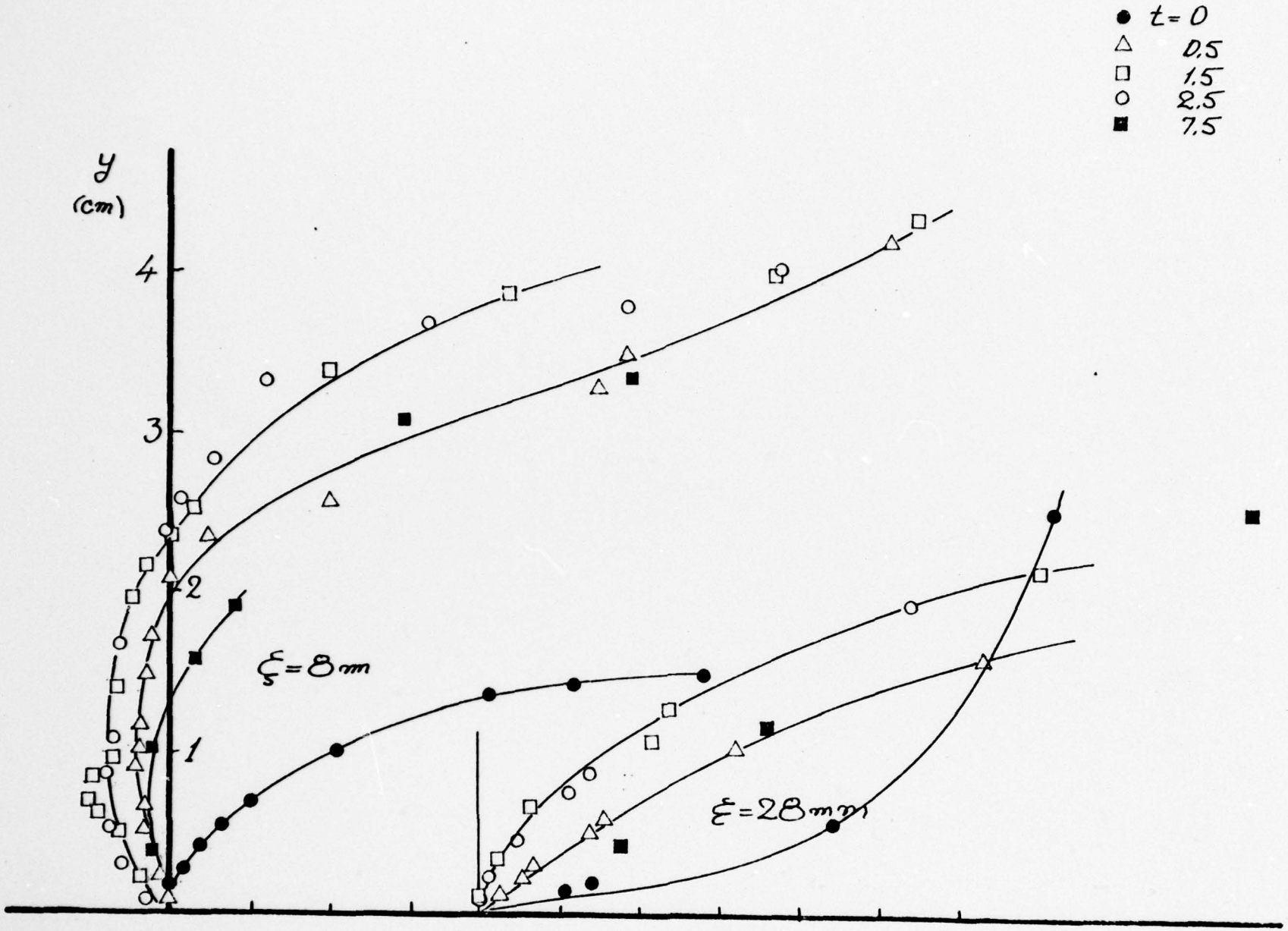

Fig. 5.7 Velocity profiles at stations ξ=8&28 (see Fig. 5.1) derived from the flow visualization of Fig. 5.6.

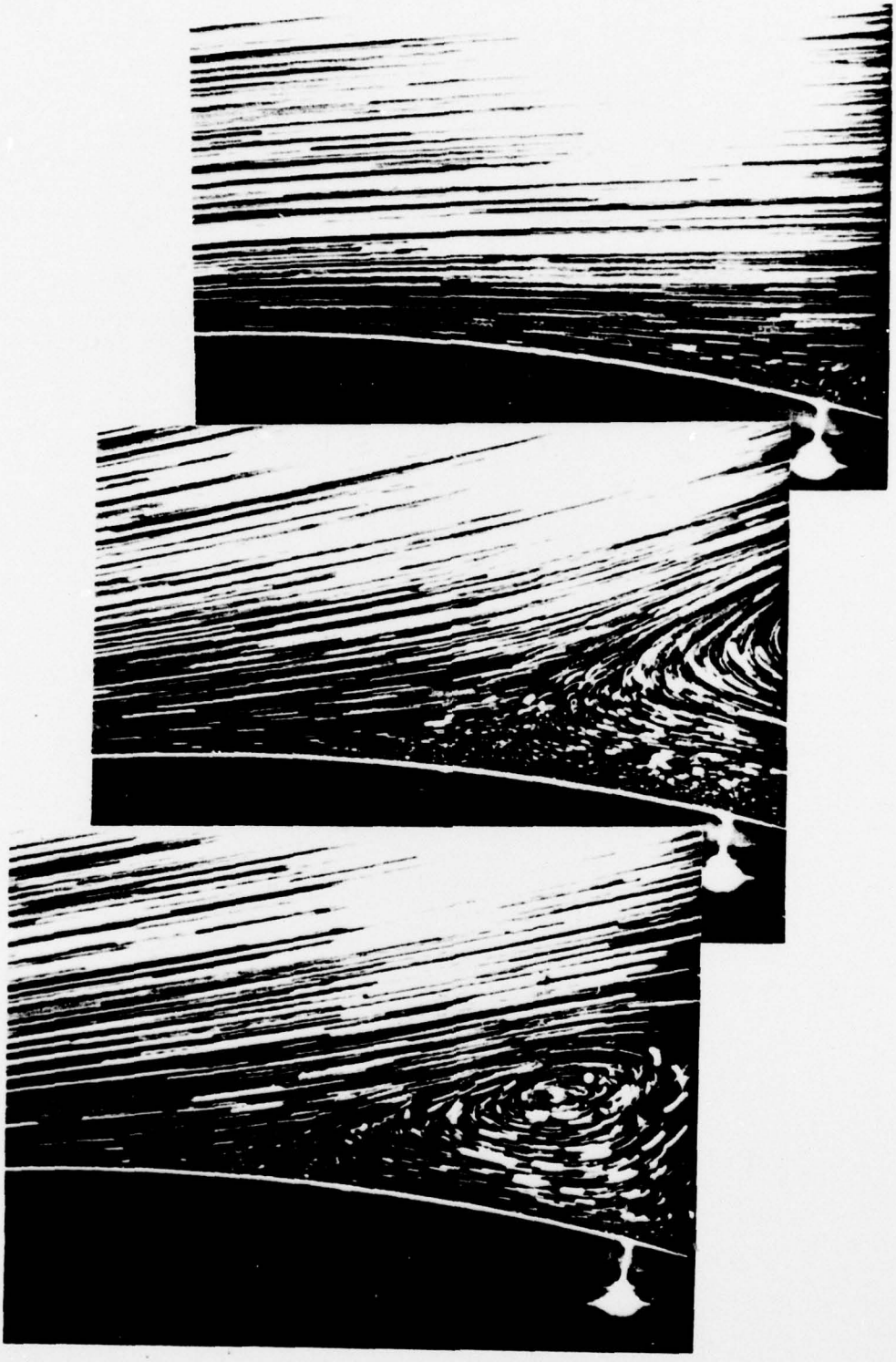

Fig. 5.8 Flow visualization of instantaneous velocity fields for an impulsive change $\theta_I = 0$ to $\theta_{II} = 30°$ and $R_e \cong 1000$

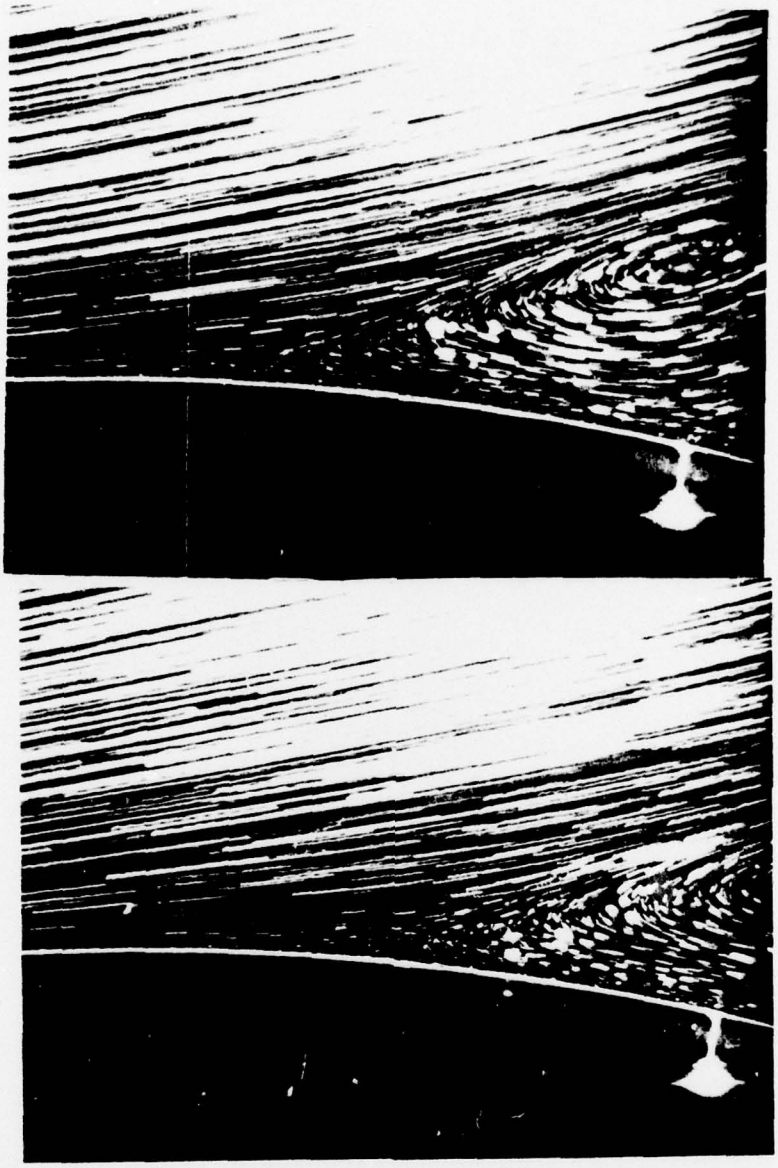

Fig. 5.8 (continued) Flow visualization of instantaneous velocity fields for an impulsive change $\theta_I = 0$ to $\theta_{II} = 30°$ and $R_e \cong 1000$

t=0

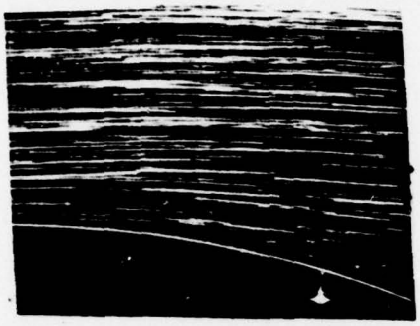

t=0.5 sec

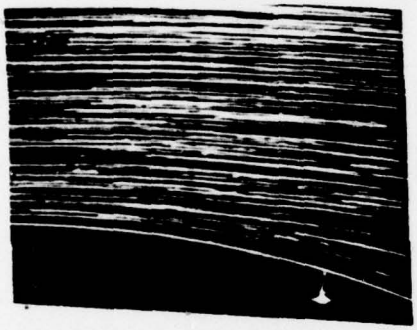

t=1.5 sec

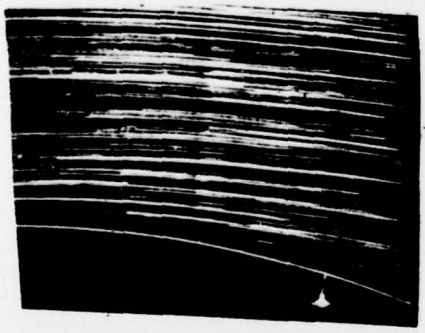

t=2.5 sec

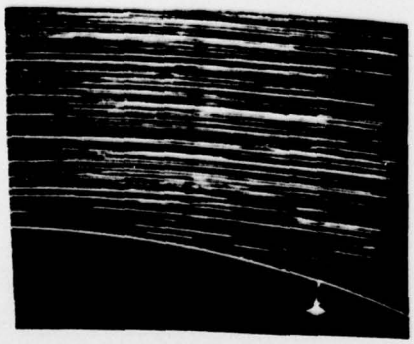

t=3.5 sec

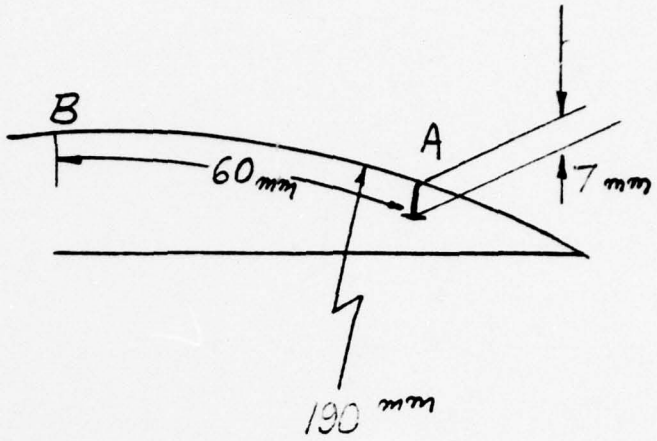

Fig a

Fig. 6.1 Flow visualization for flow accelerating in magnitude from U_∞ = 12 cm/sec. to U_∞ = 25 cm/sec.

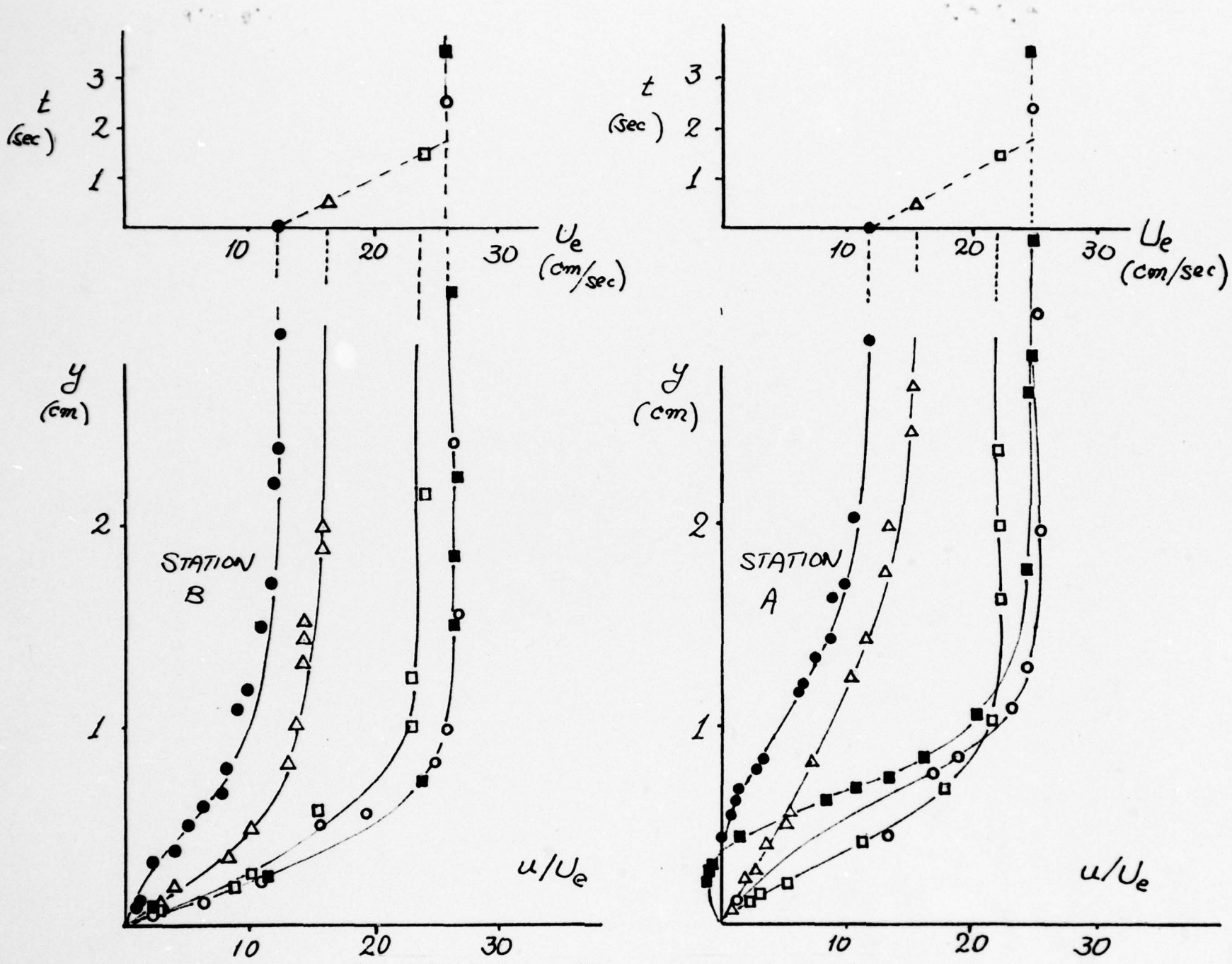

Fig. 6.2 Velocity profiles at stations A and B (see Fig. 5.1) derived from the flow visualization of Fig. 6.1

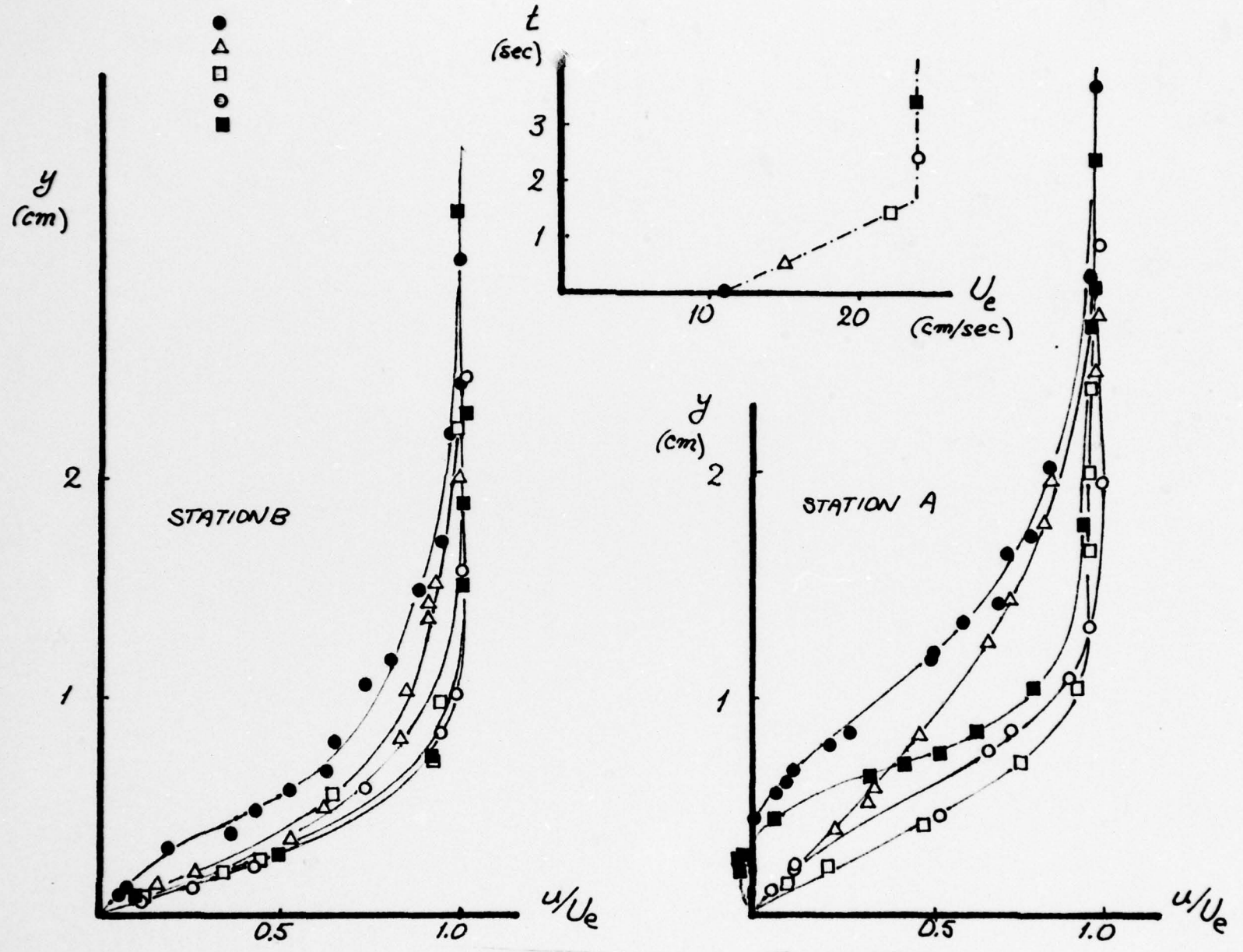

Fig. 6.3 The velocity profiles of Fig. 6.2 normalized with the outer flow velocity.

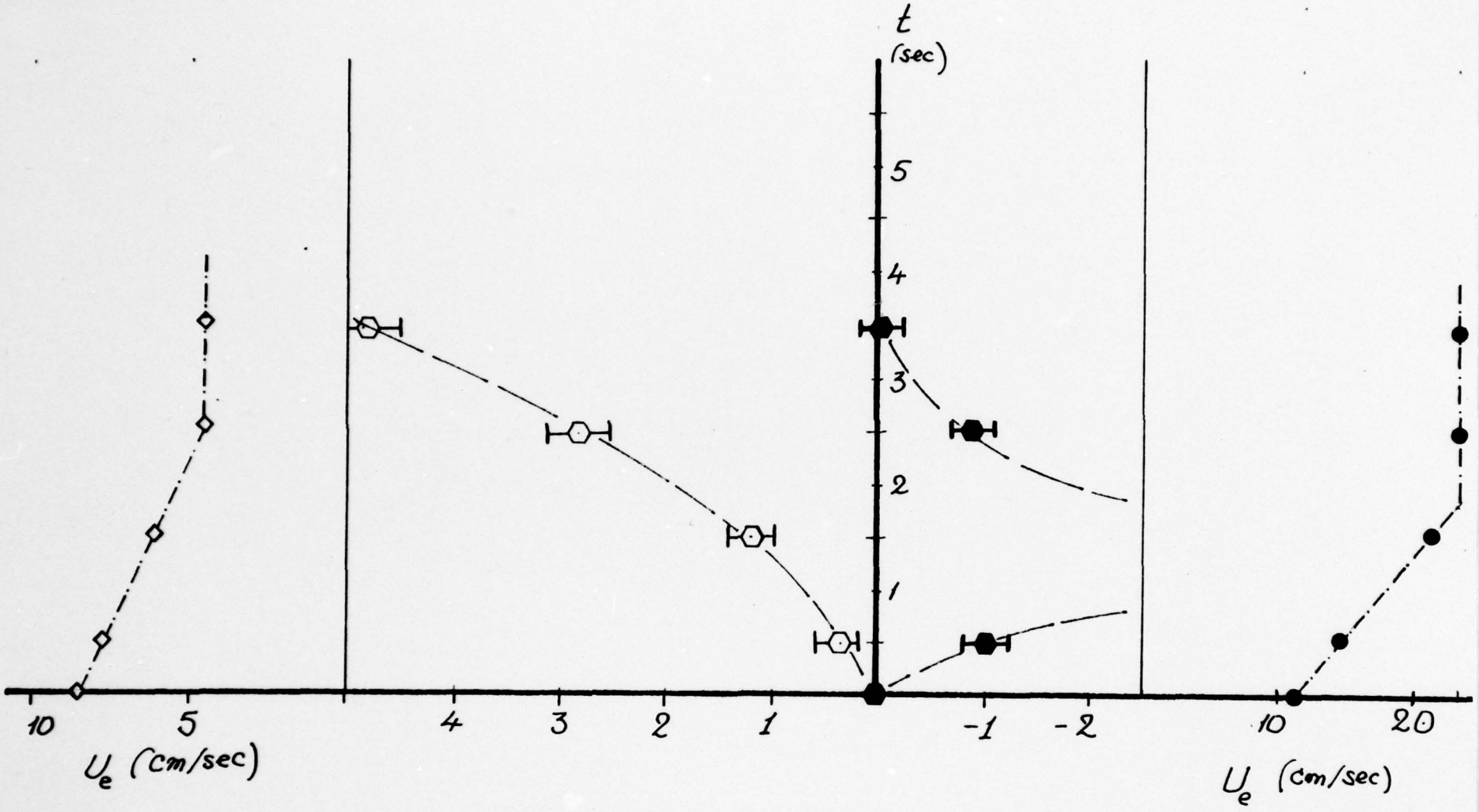

Fig. 6.4 The temporal excursions of the point of separation for flows accelerating and decelerating in magnitude. The origin is located at ξ = 8 mm (see Fig. 5.1)

Unclassified
SECURITY CLASSIFICATION OF THIS PAGE (When Data Entered)

ARO 12680.4-E

REPORT DOCUMENTATION PAGE

READ INSTRUCTIONS BEFORE COMPLETING FORM

1. REPORT NUMBER: 12680.4-E	2. GOVT ACCESSION NO.
3. RECIPIENT'S CATALOG NUMBER	
4. TITLE (and Subtitle): Experimental Investigation of Unsteady Separation	5. TYPE OF REPORT & PERIOD COVERED: Technical Report
	6. PERFORMING ORG. REPORT NUMBER
7. AUTHOR(s): D. P. Telionis, C. A. Koromilas	8. CONTRACT OR GRANT NUMBER(s): DAHC04 75 G 0067
9. PERFORMING ORGANIZATION NAME AND ADDRESS: Virginia Polytechnic Institute and State University, Blacksburg, Virginia 24061	10. PROGRAM ELEMENT, PROJECT, TASK AREA & WORK UNIT NUMBERS
11. CONTROLLING OFFICE NAME AND ADDRESS: U. S. Army Research Office, Post Office Box 12211, Research Triangle Park, NC 27709	12. REPORT DATE: January 1978
	13. NUMBER OF PAGES: 60
14. MONITORING AGENCY NAME & ADDRESS (if different from Controlling Office)	15. SECURITY CLASS. (of this report): Unclassified
	15a. DECLASSIFICATION/DOWNGRADING SCHEDULE

16. DISTRIBUTION STATEMENT (of this Report)

Approved for public release; distribution unlimited.

17. DISTRIBUTION STATEMENT (of the abstract entered in Block 20, if different from Report)

18. SUPPLEMENTARY NOTES

The findings in this report are not to be construed as an official Department of the Army position, unless so designated by other authorized documents.

19. KEY WORDS (Continue on reverse side if necessary and identify by block number)

20. ABSTRACT (Continue on reverse side if necessary and identify by block number)

This is a preliminary report on a project which essentially involves the setting up of special laboratory equipment to investigate unsteady viscous phenomena and the development of appropriate methods of visualization. The present report contains only a sample of experimental results and some initial interpretations. Much more data have been collected and is now being processed. Moreover, ~~we are in the process of generating~~ more information is being acquired beyond the schedule originally proposed. It is expected to complete this phase of the work around May of 1978 and the final report can be completed in June or July 1978.

DD FORM 1 JAN 73 1473 EDITION OF 1 NOV 65 IS OBSOLETE

Unclassified
SECURITY CLASSIFICATION OF THIS PAGE (When Data Entered)